# Phage portal proteins counteract stringent-response–mediated restriction

Kristina Kronborg[1#], Luokai Wang[1,2#], Muriel Leandra Schicketanz[1^], Kenn Gerdes[3], Yong Everett Zhang[1*]

[1] Department of Biology, University of Copenhagen, DK-2200 Copenhagen, Denmark

[2] School of Clinical and Basic Medical Sciences, Shandong First Medical University & Shandong Academy of Medical Sciences, Jinan 250117, China.

[3] Independent researcher, Copenhagen, Denmark

[#] K.K. and L.K.W. contributed equally to this work.

^ Current address: Novonesis A/S, Kgs. Lyngby, Denmark

*Correspondence: Yong Everett Zhang zhangy830328@gmail.com

Running title: Phage portal proteins as anti-stringent-response factors

**Abstract**

Bacteria restrict viral replication not only through dedicated defense systems but also by entering global physiological states that limit cellular resources. How phages counter such host-imposed physiological barriers remains poorly understood. The stringent response (SR), mediated by the alarmones ppGpp and pppGpp, induces a growth-restrictive state that can act as a barrier to bacteriophage infection. Here we show that elevated alarmone levels delay T7-mediated host lysis, whereas (p)ppGpp-deficient cells are hypersensitive to infection, establishing alarmone signaling as a physiological constraint on phage replication. A systematic functional screen identifies the essential capsid portal protein Gp8 as a viral factor genetically linked to SR-dependent host physiology. Gp8 directly binds the alarmone synthetases RelA and SpoT, selectively inhibiting their synthetase activities *in vitro* and suppressing alarmone accumulation *in vivo*. Phages carrying interaction-defective portal mutations exhibit impaired replication, delayed lysis, and sustained (p)ppGpp elevation during infection, defects that are alleviated in SR-deficient hosts. Structural and mutational analyses reveal electrostatically mediated interfaces required for targeting RelA and SpoT. Portal proteins from diverse coliphages share similar structural features, interact with stringent-response enzymes, and display SR-linked phenotypes, indicating a broadly conserved viral strategy. Together, these findings identify phage portal proteins as a previously unrecognized class of viral counter-defense factors that target a central bacterial stress signaling pathway, revealing that essential structural virion components can moonlight as regulators of host stress physiology.

**Keywords**

Bacteriophage-host interactions, phage counter-defense, stringent response, (p)ppGpp signaling, stress physiology, portal protein

41 **Introduction**

42 Bacteria employ multilayered defense networks to restrict viral infection, combining
43 dedicated systems such as restriction-modification, CRISPR-Cas, abortive infection modules,
44 and nucleotide-based immune signaling pathways with broader physiological states that limit
45 viral replication[1-4]. Whereas many antiviral mechanisms rely on molecular recognition of
46 invading phages, global physiological responses can impose resource constraints that
47 indirectly restrict infection. Physiological growth arrest, a common outcome of abortive
48 infection systems, limits phage spread by sacrificing infected cells[5]. How phages contend
49 with such host-imposed physiological barriers remains incompletely understood.

50 One of the most ancient and conserved physiological responses is the stringent response (SR),
51 mediated by the alarmones ppGpp and pppGpp[6,7]. Activation of the SR reprograms
52 transcription and metabolism, suppressing ribosome biogenesis and nucleotide synthesis
53 while promoting stress adaptation[8]. Although classically viewed as a stress-adaptation
54 mechanism, the growth-restrictive state imposed by the SR creates an intracellular
55 environment that is unfavorable for bacteriophage replication, suggesting that it can function
56 as a physiological barrier to infection.

57 Consistent with this view, (p)ppGpp signaling influences bacteriophage infection outcomes.
58 Cells lacking alarmone synthesis are hypersensitive to phage killing, whereas stationary-
59 phase cells, characterized by elevated alarmone levels, often exhibit increased resistance[9-11].
60 Toxic Rel-family proteins have also emerged in multiple abortive infection systems[12-15],
61 underscoring the recurrent involvement of RSH-associated regulatory pathways in phage–
62 host interactions. Conversely, certain phage-encoded factors, such as the alarmone-degrading
63 enzyme ATD1[16], directly modulate (p)ppGpp metabolism during infection. Together, these

64 observations indicate that alarmone-linked stress networks are repeatedly engaged during
65 defense and counter-defense processes.

66 Phages, in turn, have evolved diverse strategies to neutralize host defenses, including
67 inhibitors of CRISPR-Cas systems, restriction enzymes, abortive infection pathways, and
68 cyclic-nucleotide immune signaling modules[17,18]. Most characterized anti-defense factors
69 target discrete molecular effectors. Whether phages also encode dedicated mechanisms to
70 counteract global physiological restriction states, such as the SR, remains largely unexplored.
71 Because the SR is governed by a small number of conserved enzymes, it represents a
72 potentially vulnerable node for viral counter-defense.

73 In *Escherichia coli*, the SR is mediated primarily by the (p)ppGpp synthetases RelA and
74 SpoT[19-23]. Elevated alarmone levels remodel transcription through direct interactions with
75 RNA polymerase (RNAP)[24,25], limiting biosynthetic capacity and slowing growth[26-28].
76 Although this reprogramming enhances stress survival, it may also constrain the metabolic
77 demands of phage replication. Consistent with this, bacteriophage T7 encodes multiple
78 inhibitors of host RNAP[11,29-31], highlighting the importance of transcriptional control during
79 infection. These observations raise the possibility that phages actively modulate SR signaling
80 to optimize infection.

81 Here, we investigate the interplay between the SR and infection by bacteriophage T7. Using
82 complementary genetic, biochemical, and phage mutational approaches, we identify the
83 essential T7 capsid portal protein Gp8 as a direct inhibitor of (p)ppGpp synthesis. Gp8
84 physically interacts with RelA and SpoT, selectively suppressing their synthetase activities
85 and reducing intracellular alarmone accumulation during infection. Disruption of this
86 interaction impairs phage replication and delays host lysis. Portal proteins from diverse *E.*
87 *coli* phages exhibit similar properties, revealing a broadly conserved strategy by which

88 structural virion components moonlight as modulators of host stress physiology to promote
89 infection.

90 **Results**

91 **The stringent response limits bacteriophage infection**

92 Bacterial stress responses reshape cellular physiology in ways that can influence
93 susceptibility to viral infection. To test whether the stringent response (SR) affects
94 bacteriophage replication, we examined infection by bacteriophage T7 in a (p)ppGpp$^0$
95 *Escherichia coli* strain lacking both *relA* and *spoT*. Compared with wild-type cells, the
96 alarmone-deficient host exhibited accelerated killing kinetics and more rapid lysis, as
97 reflected by larger plaque sizes and increased plaque expansion rates (**Fig. 1a,b**). These
98 results indicate that loss of alarmone signaling enhances phage infection, consistent with
99 previous report[11].

100 We next tested whether elevated alarmone levels have the opposite effect. Strains carrying
101 *spoT* alleles that increase basal (p)ppGpp concentrations (*spoT202* and *spoT203*)[32,33]
102 displayed delayed lysis kinetics relative to *spoT* wild-type allele cells, characterized by
103 prolonged lag phases prior to host population collapse and reduced lysis slopes (**Fig. 1c**).
104 Across genetic backgrounds, higher intracellular alarmone levels were associated with slower
105 infection progression.

106 Together, these results demonstrate that alarmone signaling establishes a growth-restrictive
107 intracellular environment that limits bacteriophage replication. The SR therefore functions as
108 a physiological barrier to infection, suggesting that successful phages must encode
109 mechanisms to overcome this defense-associated state.

110 **T7 encodes factors that interfere with stringent-response-dependent host physiology**

111 Because elevated alarmone levels restrict phage infection (**Fig. 1**), we reasoned that T7 may
112 encode factors that counteract the SR-associated physiological state. Anti-defense systems
113 often manifest as proteins that perturb host pathways required specifically under stress or
114 nutrient-limited conditions. We therefore performed a systematic functional screen to identify
115 T7 proteins that interfere with host growth under conditions in which (p)ppGpp signaling is
116 required.

117 We cloned 53 T7 genes under the arabinose inducible control of the pBAD33 vector and
118 assessed their effects on *E. coli* growth in rich (LB) and minimal media (M9) (**Fig. 2a**).
119 Strikingly, 34 of 53 T7 proteins caused severe growth inhibition when expressed in minimal
120 medium, whereas most exhibited little or no toxicity in rich medium (**Fig. 2b**; Supplementary
121 **Fig. S1**). This conditional toxicity pattern suggests that T7 encodes numerous factors
122 targeting host processes that become critical under nutrient limitation, a physiological context
123 strongly influenced by alarmone signaling.

124 To identify T7 proteins specifically linked to SR-dependent physiology, we next exploited
125 RNA polymerase (RNAP) mutants with a stringent-like ($RNAP^{SR}$) phenotype that bypass the
126 requirement for (p)ppGpp during growth in minimal medium[34,35]. Expression of four T7
127 proteins, Gp1.5, Gp4.2, Gp6.5, and Gp8, showed reproducible suppression of toxicity in two
128 independent $RNAP^{SR}$ backgrounds (Supplementary **Fig. S2-S3**). Notably, suppression
129 persisted in a (p)ppGpp$^{0}$ strain carrying the $RNAP^{SR}$ allele[34] (**Fig. 2c)**, indicating that rescue
130 does not require alarmone synthesis itself but rather depends on SR-regulated transcriptional
131 programs.

132 Together, these results identify a subset of T7 proteins genetically linked to host SR
133 pathways, consistent with the presence of viral factors that interfere with this defense-
134 associated physiological state.

135 **The portal protein Gp8 directly targets the alarmone synthetases RelA and SpoT**

136 The genetic link between a subset of T7 proteins and SR-dependent host physiology
137 prompted us to test whether these candidates directly target components of the alarmone
138 signaling machinery. We therefore examined physical interactions between Gp1.5, Gp4.2,
139 Gp6.5, and Gp8 and the central SR regulators RelA, SpoT, and RNAP (i.e., the ω subunit
140 RpoZ) using a bacterial two-hybrid assay. Among the proteins tested, the T7 portal protein
141 Gp8 showed robust and reproducible interactions with both RelA and SpoT (**Fig. 3a**),
142 whereas the other candidates did not display consistent interactions.

143 We validated these associations biochemically by co-purification assays using Flag-tagged
144 Gp8 and His-MBP-SUMO(HMS)-tagged RelA or SpoT. In both cases, Gp8 specifically
145 copurified with the alarmone synthetases, confirming direct physical interaction *in vitro* (**Fig.**
146 **3b**). These results identify Gp8, an essential structural component of the T7 capsid portal
147 vertex, as a viral protein that directly engages the core enzymatic machinery responsible for
148 (p)ppGpp synthesis.

149 We next asked whether Gp8 binding affects the catalytic activities of RelA and SpoT. *In vitro*
150 enzymatic assays revealed that Gp8 potently inhibited the synthetase activities of both
151 enzymes in a dose-dependent manner (**Fig. 3c**). In contrast, Gp8 had no detectable effect on
152 the hydrolase activity of SpoT (**Fig. 3d**), indicating that the portal protein selectively
153 suppresses alarmone synthesis rather than globally perturbing SpoT function. Consistent with
154 this, expression of Gp8 *in vivo* suppressed intracellular (p)ppGpp accumulation relative to
155 control conditions (**Fig. 3e** and Supplementary **Fig. S3**).

156 Together, these findings demonstrate that the phage portal protein Gp8 directly binds and
157 inhibits the alarmone synthetases RelA and SpoT, revealing a mechanism by which T7
158 suppresses the SR pathway.

159 **Electrostatic interfaces on the portal ring mediate targeting of RelA and SpoT**

160 Gp8 assembles into a dodecameric ring that forms the portal vertex of the T7 capsid, with
161 exterior surfaces enriched in charged residues (**Fig. 4a**). To define the regions of Gp8
162 required for interaction with RelA and SpoT, we generated domain truncations and assessed
163 binding using the bacterial two-hybrid assay. Deletion of either the N- or C-terminal regions
164 of Gp8 abolished interactions with both RelA and SpoT, whereas removal of the clip domain
165 reproducibly enhanced interaction signals. Further deletion extending into the stem domain
166 eliminated binding entirely (**Fig. 4b**). These results indicate that an intact portal ring
167 architecture is required for targeting the alarmone synthetases and suggest that the clip motif
168 does not itself contribute to binding but instead modulates access to the interaction surface.

169 Notably, the clip motif is enriched in positively charged residues, whereas the remainder of
170 the portal exterior is predominantly electronegative (**Fig. 4a**). The observation that deletion of
171 a positively charged element enhances binding suggests that RelA and SpoT preferentially
172 engage negatively charged surfaces on the assembled portal ring and that the clip motif may
173 partially shield or sterically constrain these interfaces in the intact protein. We therefore
174 tested whether electrostatic interactions underlie RelA/SpoT binding by generating 43
175 charge-reversal mutants targeting clusters of surface-exposed acidic and basic residues.

176 Approximately half of the charge-reversal mutants exhibited substantial loss of interaction
177 with RelA, and the same substitutions similarly impaired SpoT binding (**Fig. 4c** and
178 Supplementary **Fig. S4a-e**). Several mutations - including D220R/E221R, D457K/D460K,

179 E280R/E284R, K4D/R5D, and K288D/K295D - abolished interaction entirely, identifying
180 discrete charged surface patches (**Fig. 4a)** that are jointly required for targeting both
181 enzymes. These results support a model in which RelA and SpoT recognize a defined
182 electrostatic landscape on the portal ring.

183 To define the corresponding interfaces on the host proteins, we performed domain mapping
184 of RelA and SpoT. Removal of the N-terminal catalytic domains of SpoT eliminated its
185 interaction with Gp8, whereas truncation of the C-terminal regulatory domains of RelA
186 disrupted binding (**Fig. 4d** and Supplementary **Fig. S4f,g**). Thus, Gp8 engages RelA and
187 SpoT through distinct domain interfaces, while relying on a common set of electrostatically
188 defined surfaces on the portal ring.

189 Together, these data demonstrate that the portal protein uses a spatially organized pattern of
190 surface charges to target the alarmone synthesis machinery, supporting the idea that
191 suppression of the SR reflects a specific, evolved molecular interaction rather than a
192 secondary consequence of portal assembly.

193 **Suppression of alarmone signaling by Gp8 is required for efficient phage infection**

194 To determine whether Gp8-mediated targeting of RelA and SpoT contributes to phage
195 fitness, we generated T7 phages carrying portal mutations that disrupt interaction with the
196 alarmone synthetases. Using recombineering, we isolated mutant phages bearing substitutions
197 D220R/E221R (interaction-defective) and E10K/D11K (partially defective), and confirmed
198 impaired binding to RelA and SpoT by pull-down assays (**Fig. 5a**).

199 In plaque assays on wild-type *E. coli*, the interaction-defective mutant formed significantly
200 smaller plaques than $T7_{wt}$, whereas the partially defective mutant displayed an intermediate
201 phenotype (**Fig. 5b,c**). These defects were alleviated in hosts lacking SR signaling: plaque

202 sizes increased in Δ*relA* cells for the partially defective mutant and in (p)ppGpp$^0$ cells for all
203 phages tested, indicating that impaired infection is linked to the host alarmone pathway.

204 We next quantified infection dynamics in liquid culture at a multiplicity of infection (MOI) of
205 0.1. Compared with $T7_{wt}$, the interaction-defective mutant exhibited a marked delay in host
206 cell lysis during infection of wild-type cells (**Fig. 5d**). This delay was substantially reduced in
207 Δ*relA* and nearly abolished in (p)ppGpp$^0$ strains, demonstrating that elevated alarmone levels
208 are responsible for much of the infection defect (**Fig. 5d**). This is consistent with the prior
209 observation that hosts with genetically elevated basal (p)ppGpp levels displayed delayed lysis
210 (**Fig. 1b**), supporting an inverse relationship between alarmone abundance and infection
211 efficiency.

212 To directly monitor alarmone dynamics during infection, we radiolabeled intracellular
213 nucleotide pools and quantified (p)ppGpp levels over time. Because complex media such as
214 LB interfere with nucleotide labeling, these experiments were performed in defined MOPS
215 medium. Importantly, the relative infection phenotypes observed in LB were preserved under
216 these conditions, with wild-type T7 lysing *E. coli* more rapidly than the interaction-defective
217 mutant (Supplementary **Fig. S7a**).

218 Infections were performed at the same MOI of 0.1, such that population-wide lysis requires at
219 least two rounds of infection, and alarmone dynamics are most clearly resolved during the
220 first, relatively synchronized infection cycle. During this initial cycle, infection with the
221 interaction-defective T7 mutant resulted in sustained elevation of (p)ppGpp prior to the onset
222 of lysis, whereas alarmone levels were markedly reduced during wild-type T7 infection (**Fig.
223 5e** and Supplementary **Fig. S7b,c**). Elevated (p)ppGpp levels coincided with pronounced
224 depletion of GTP and ATP pools, consistent with SR-associated repression of nucleotide
225 biosynthesis[36-39]. At later time points corresponding to subsequent infection cycles and final

226 population collapse, differences in alarmone levels between wild-type and mutant infections
227 were diminished, likely reflecting increased heterogeneity in infection timing following the
228 first lysis event.

229 Together, these results indicate that portal-mediated suppression of alarmone signaling
230 promotes efficient T7 infection and that disruption of the Gp8-RelA/SpoT interaction leads to
231 sustained SR activation and delayed infection progression.

232 **Portal-mediated suppression of the stringent response is conserved among coliphages**

233 Gp8 is an essential structural component of the phage capsid and is widely conserved among
234 tailed bacteriophages. To determine whether portal-mediated targeting of the SR represents a
235 broader viral strategy, we examined portal proteins from phylogenetically diverse *E. coli*
236 phages in the BASEL collection[40]. Structural predictions indicated that many of these portal
237 proteins assemble into ring-like complexes with predominantly electronegative exterior
238 surfaces, similar to that of T7 Gp8 (**Fig. 6a**; Supplementary Document 2).

239 Consistent with a general role for the stringent response in restricting infection, many of these
240 phages infected (p)ppGpp$^0$ cells more efficiently than wild-type hosts, producing larger or
241 clearer plaques or increased plaque-forming units (**Fig. 6b**; Supplementary Document 2).
242 Notably, portal proteins from these phages also displayed a conserved pattern of surface
243 charge segregation, with negatively charged exterior regions juxtaposed to discrete positively
244 charged elements (**Fig. 6a**), suggesting that this electrostatic organization may be a common
245 feature associated with SR sensitivity.

246 To test whether portal proteins with this charge organization directly engage the alarmone
247 synthesis machinery, we focused on representatives from two unrelated coliphages, P1 and
248 N4. Although these phages differ substantially in genome organization, replication strategy,

249 and virion architecture, their portal proteins form dodecameric ring assemblies analogous to
250 that of T7 Gp8. In both cases, the portal proteins displayed a nonuniform surface charge
251 distribution characterized by a positively charged clip-like region juxtaposed to a
252 predominantly electronegative exterior surface (**Fig. 6a**). Expression of the P1 and N4 portal
253 proteins was toxic in *E. coli* under conditions requiring SR function, and this toxicity was
254 partially suppressed by $RNAP^{SR}$ alleles (Supplementary **Fig. S8**). In bacterial two-hybrid
255 assays, both portal proteins interacted with RelA and SpoT (**Fig. 6c**).

256 Together, these results demonstrate that portal proteins from evolutionarily distinct
257 coliphages share conserved surface charge features and the capacity to interact with the
258 alarmone synthesis machinery, indicating that portal-mediated modulation of stringent-
259 response signaling is not unique to bacteriophage T7.

## 260 Discussion

### 261 A conserved role for phage portal proteins in repression of the stringent response

262 Together, these findings indicate that the SR can function not only as a stress adaptation
263 pathway but also as a physiological barrier that constrains phage replication. While the SR
264 has long been recognized for its role in bacterial survival under nutrient limitation and
265 environmental stress, its capacity to globally suppress biosynthesis, transcription, and
266 nucleotide availability also creates an intracellular environment that is unfavorable for viral
267 replication. In contrast to dedicated antiviral defense systems that rely on molecular
268 recognition of invading phages, the SR represents a distinct mode of host defense: rather than
269 detecting phage components directly, it enforces a system-level physiological state that
270 indirectly restricts viral growth by limiting access to essential cellular resources. Such global

271 restriction mechanisms may be particularly effective against diverse phages, as they do not
272 depend on specific recognition motifs that can be readily mutated or evaded.

273 **A biphasic model for SR modulation during T7 infection**

274 Based on our data, we propose a biphasic model for the role of (p)ppGpp during T7 infection
275 (**Fig. 7**). Early in infection, phage invasion and host takeover trigger stress responses that
276 activate (p)ppGpp synthesis. At this stage, suppression of host metabolism, particularly
277 inhibition of host RNAP, is advantageous to the phage, as it limits competing cellular
278 processes and facilitates the transition to phage-directed transcription[41]. Notably, (p)ppGpp
279 preferentially inhibits *E. coli* RNAP while having little effect on T7 RNAP[42,43], allowing
280 phage transcription to proceed efficiently. This effect is reinforced by multiple T7-encoded
281 inhibitors of host RNAP (Gp2[29,31], Gp5.7[11], Gp0.7[30]), underscoring the importance of early
282 host transcriptional shutdown for productive infection[41].

283 As infection progresses, however, the physiological requirements of the phage shift. Late
284 stages of infection involve massive synthesis of structural proteins and energy-intensive
285 genome packaging by the terminase-portal complex, processes that place high demands on
286 cellular amino acids and nucleotide pools[44,45]. Uncontrolled (p)ppGpp accumulation becomes
287 detrimental at this stage, as it depletes ATP and GTP and further suppresses their
288 biosynthesis[36-39]. Our data indicate that Gp8-mediated inhibition of RelA and SpoT alleviates
289 this constraint by suppressing (p)ppGpp levels prior to lysis, thereby restoring nucleotide
290 availability and enabling efficient virion assembly and release.

291 In this framework, the portal protein functions as a molecular gatekeeper that coordinates the
292 transition from early host metabolic repression to late-stage resource mobilization, ensuring
293 optimal timing of lysis and maximal phage yield. This biphasic control highlights how phages

294 not only tolerate host defense-associated stress responses but actively repurpose them to
295 optimize different phases of their replication cycle.

296 **Evolutionary implications of portal proteins as anti-defense factors**

297 The identification of a regulatory role for the phage portal protein is evolutionarily striking.
298 Portal proteins are among the most conserved and structurally constrained components of
299 tailed phages, forming the central channel through which viral DNA is packaged and later
300 delivered into the host. Their essential architectural role would be expected to limit sequence
301 plasticity and functional diversification. Nonetheless, our data reveal that portal proteins have
302 evolved spatially organized, electrostatically defined surface features capable of engaging
303 host regulatory enzymes and modulating global signaling pathways. This suggests that strong
304 selective pressure has favored coupling of genome delivery and packaging machinery with
305 mechanisms that suppress host stress physiology. Such multifunctionality may ensure that
306 evasion of host physiological restriction is tightly coordinated with late-stage replication
307 demands, minimizing the risk that host defenses interfere with energetically costly assembly
308 and packaging processes. More broadly, these findings expand the conceptual scope of phage
309 anti-defense strategies by demonstrating that essential structural virion components - not only
310 small, dedicated inhibitors - can moonlight as modulators of host stress physiology.

311 **Multifunctional phage proteins and conditionally essential host processes**

312 The identification of a regulatory role for the portal protein highlights a broader principle in
313 phage biology: the evolution of multifunctional proteins that target host processes essential
314 under specific physiological conditions. Such functional layering is not unique to Gp8. For
315 example, T7 lysozyme (Gp3.5) not only mediates host cell lysis but also regulates T7 RNAP

316 to coordinate transcription and replication[46,47]. These dual-purpose proteins enable phages to
317 maximize functional output from compact genomes.

318 Consistent with this idea, our functional screens revealed numerous T7 proteins that are toxic
319 specifically under nutrient-limited conditions but not in rich media. This conditional toxicity
320 suggests that phages encode factors targeting host pathways that become essential during
321 stress, a context frequently encountered in natural and clinical environments but rarely
322 captured in standard laboratory assays. As bacteria in nature often reside in nutrient-poor or
323 otherwise stressful niches, phage strategies that exploit stress-adapted host physiology are
324 likely widespread and ecologically relevant.

325 **Broader implications and future directions**

326 The identification of RSH-family toxins such as CapRel in abortive infection systems[12-15]
327 further underscores the recurrent involvement of alarmone-linked regulatory pathways in
328 phage–host interactions. In these systems, perturbation of translational and nucleotide
329 homeostasis leads to abortive infection outcomes, whereas our findings reveal a
330 complementary viral strategy in which phage portal proteins suppress RelA- and SpoT-
331 mediated (p)ppGpp synthesis during productive infection. Together, these observations
332 suggest that alarmone metabolism constitutes a regulatory interface engaged by both bacterial
333 defense modules and phage countermeasures.

334 Although our analysis focuses primarily on coliphages, the SR is universal across bacterial
335 phyla, raising the possibility that alarmone signaling may represent a widespread target for
336 viral counter-defense strategies. It remains to be determined whether portal-mediated
337 suppression of (p)ppGpp synthesis extends beyond enterobacterial phages. Moreover, while
338 our biochemical data demonstrate selective inhibition of RelA and SpoT synthetase activity,

339 the precise molecular mechanisms underlying this inhibition - such as whether it involves
340 allosteric regulation or steric occlusion - remain to be resolved. Finally, because (p)ppGpp
341 signaling intersects with multiple defense systems and stress-response pathways, suppression
342 of the SR may indirectly influence other layers of bacterial defense. Dissecting these
343 interactions will be an important avenue for future work aimed at understanding how global
344 physiological defenses integrate into the broader phage-host arms race.

## Figures and Legends

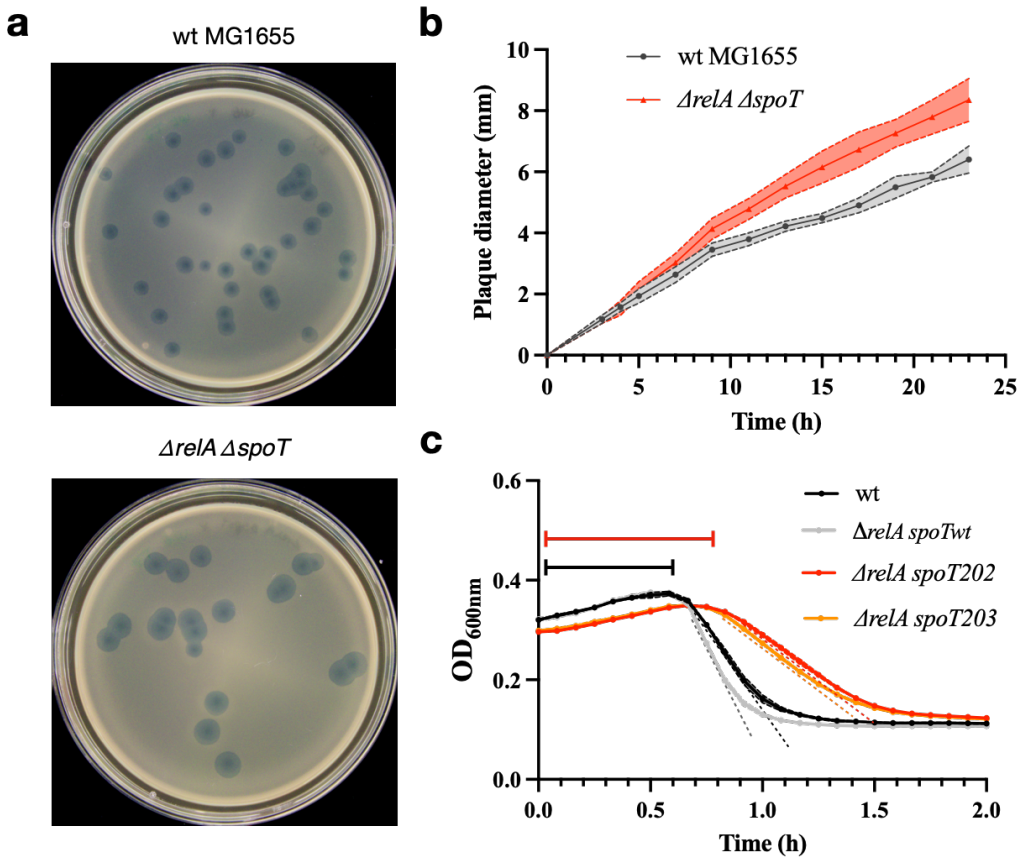


**Figure 1. The stringent response restricts bacteriophage infection.**

**a**, Plaques of T7 phage after 24-hour infection of wild-type and (p)ppGpp⁰ (*ΔrelA ΔspoT*) *Escherichia coli* on LB medium.

**b**, Quantification of plaque expansion kinetics for T7 infection of wild-type and (p)ppGpp⁰ (*ΔrelA ΔspoT*) cells, as in **a**. Data represent mean ± s.d. from five independent plaques per strain.

**c**, Lysis kinetics of wild-type MG1655, *ΔrelA spoT*wt and high-(p)ppGpp strains (*ΔrelA spoT202* and *ΔrelA spoT203*) during T7 infection. Data represent mean values from independent biological replicates; shaded areas indicate s.d.. The lag phase preceding lysis and the lysis rate (slope) are indicated.

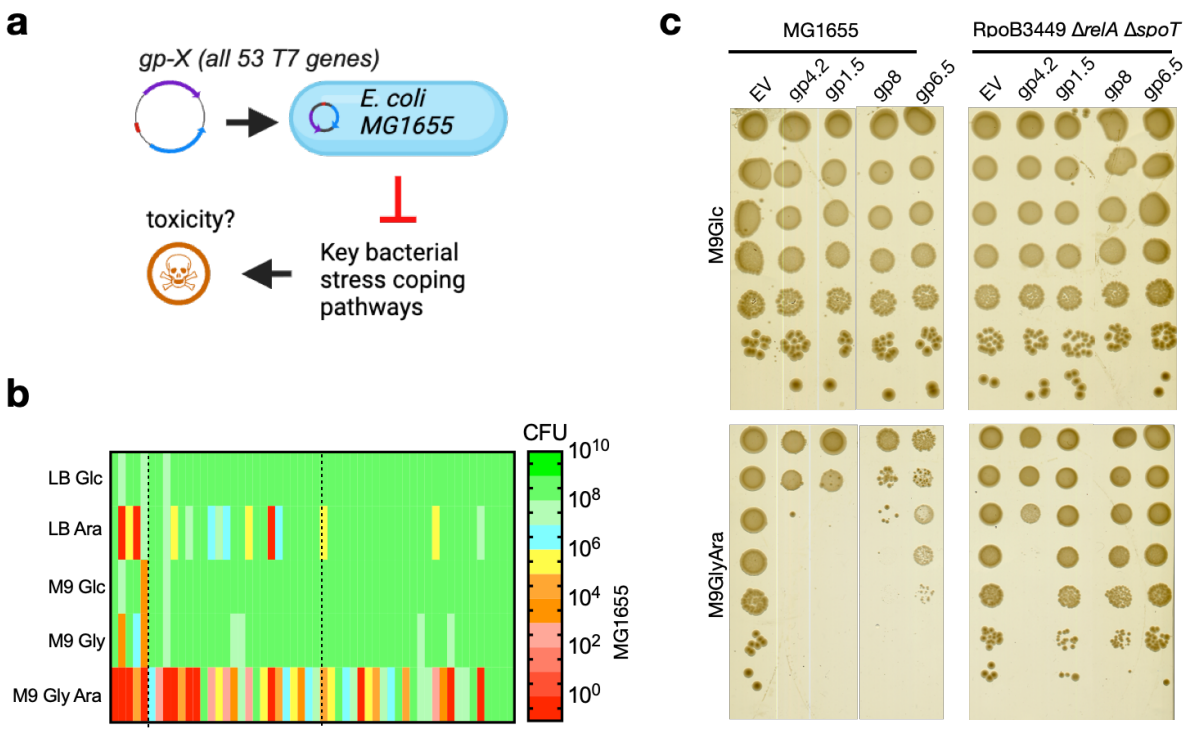


**Figure 2. Identification of T7 proteins linked to stringent-response-dependent physiology.**

**a**, Schematic of the systematic testing of all 53 phage T7 genes into the inducible plasmid vector pBAD33 and their expression in *Escherichia coli* MG1655 to screen for phage proteins that impair bacterial growth under conditions requiring stringent-response function. (Created with BioRender.com)

**b**, Growth of *E. coli* expressing individual T7 genes in rich and minimal media, quantified as CFU $ml^{-1}$ normalized to $OD_{600nm}$. LB Glc and LB Ara are LB media supplemented with 0.2% glucose and 0.2% arabinose, respectively. M9 Glc, M9 Gly, and M9 Gly Ara denote M9 minimal media supplemented with 0.4% glucose, 0.4% glycerol, or 0.4% glycerol plus 0.2% arabinose, respectively. Original plate-based growth assays are shown in **Supplementary Fig. S1**.

**c**, Suppression of T7 protein-induced growth defects in (p)ppGpp$^0$ (*ΔrelA ΔspoT*) strains carrying stringent-like RNA polymerase allele (*rpoB*3449; RNAP$^{SR}$). Serial dilutions of the indicated strains expressing gp1.5, gp4.2, gp6.5, gp8, or empty vector are shown.

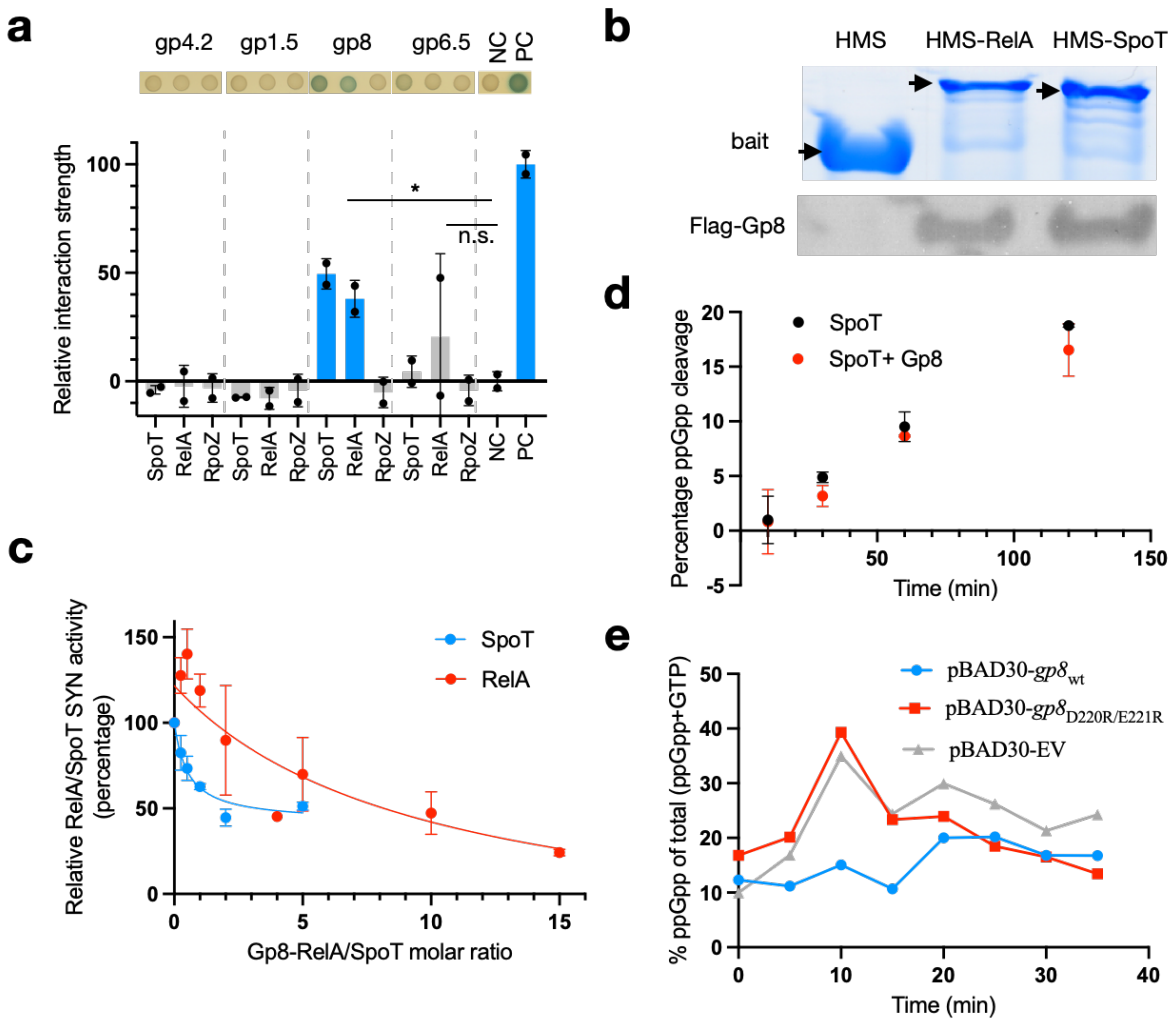


**Figure 3. The portal protein Gp8 inhibits the alarmone synthetases RelA and SpoT.**

**a**, Bacterial two-hybrid assays testing interactions between T7 proteins and RelA, SpoT, or RpoZ (the ω subunit of RNA polymerase). Data represent mean ± s.d. from two independent experiments. NC and PC denote negative and positive controls, respectively. * indicates $P < 0.05$ by Student's *t*-test. Representative spots are shown above the corresponding bars.

**b**, Pull-down assays showing co-purification of Flag-Gp8 with His-MBP-SUMO (HMS)-tagged RelA or SpoT, or with the HMS tag alone. Arrows indicate bands corresponding to the bait proteins.

**c**, *In vitro* (p)ppGpp synthetase activity of RelA and SpoT in the presence of increasing molar ratios of Gp8. Data represent mean ± s.d. from three independent experiments.

**d**, SpoT hydrolase activity measured in the absence or presence of Gp8. Data represent mean ± s.d. from two independent experiments.

**e**, Intracellular ppGpp levels, normalized to total (ppGpp + GTP), following Gp8 expression

387 from the pBAD30 vector, measured by thin-layer chromatography. EV, empty vector control.

388

389

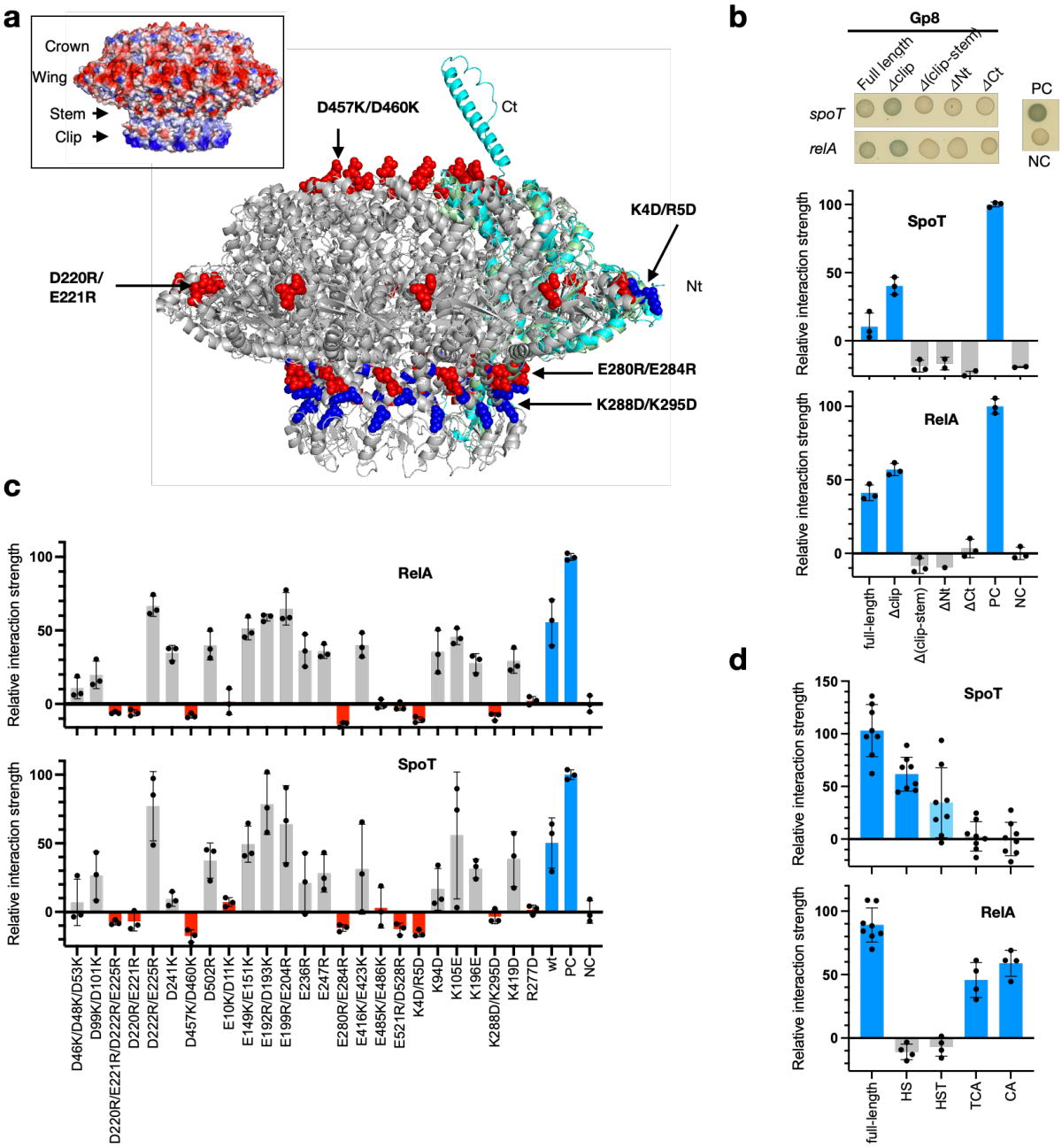


390

391 **Figure 4. Portal surface charge interfaces mediate interaction with RelA and SpoT.**
392 **a**, Structure of the T7 Gp8 portal ring (grey ribbon model; PDB 7EY6). An AlphaFold model
393 of the full-length Gp8 monomer (cyan) is overlaid with a single monomer from the portal
394 ring structure (green) to indicate the positions of the N- and C-terminal regions, including the
395 mutated K4 and R5 residues. Residues whose mutation abolished interaction with RelA and
396 SpoT are shown as spheres and labeled. Negatively charged residues are shown in red and

397 positively charged residues in blue. Inset: electrostatic surface representation of the Gp8
398 portal ring.
399
400 **b**, Bacterial two-hybrid assays assessing interactions between Gp8 truncation variants and
401 full-length RelA or SpoT. Δclip, deletion of residues 299-330; Δ(clip-stem), deletion of
402 residues 269-355; ΔNt, deletion of residues 6-42; ΔCt, deletion of residues 484-543. NC and
403 PC denote negative and positive controls, respectively. Bar plots show quantification of
404 relative interaction strengths, normalized to the positive control (PC). NC corresponds to cells
405 carrying empty vectors.
406 **c**, Quantification of relative interaction strengths between Gp8 point mutants and RelA or
407 SpoT in bacterial two-hybrid assays, normalized to the positive control (PC). NC indicates
408 negative control cells containing empty vectors. WT denotes interactions with the respective
409 wild-type RelA or SpoT proteins. Data represent means from three independent replicates.
410 Red bars indicate Gp8 mutants that completely lost interaction with both RelA and SpoT.
411 Representative raw spot images are shown in Supplementary **Fig.** S4.
412
413 **d**, Quantification of relative interaction strengths between Gp8 and truncated variants of
414 RelA or SpoT, normalized to the respective full-length proteins. Representative data from at
415 least four independent replicates are shown. Domain abbreviations: HST, hydrolase-
416 synthetase-TGS domains; HS, hydrolase-synthetase domains; TCA, TGS-CC-ACT domains;
417 CA, CC-ACT domains. Precise domain boundaries of the RelA and SpoT truncations, along
418 with representative raw spot images, are provided in Supplementary **Fig.** S4.

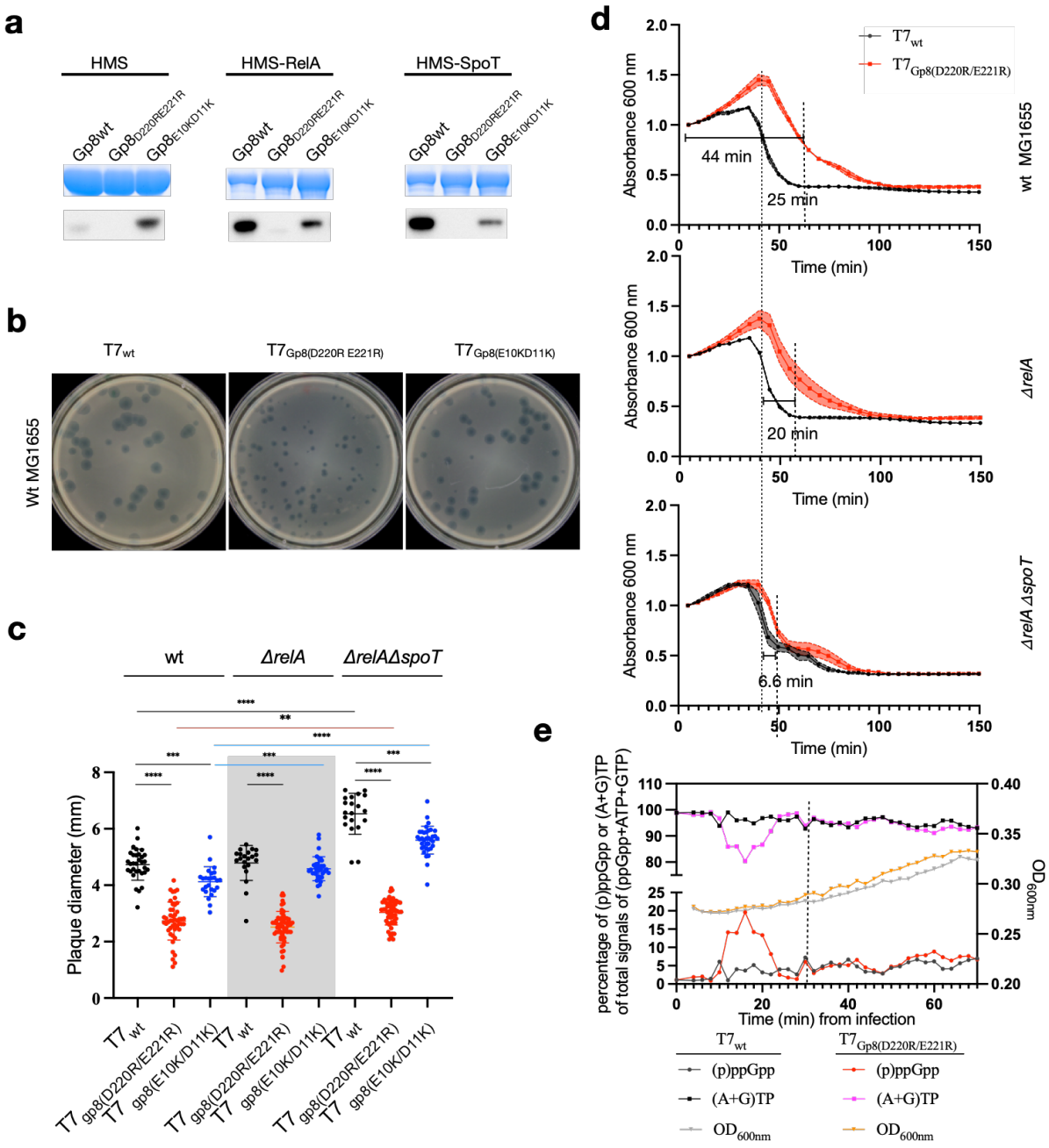


**Figure 5. Portal-mediated suppression of alarmone signaling is required for efficient infection.**

**a**, Pull-down assays using HMS-tag, HMS-RelA, or HMS-SpoT as bait with Flag-tagged wild-type (WT) or mutant Gp8 proteins. Top: SDS-PAGE analysis of the bait proteins; bottom: immunoblot detection of co-purified Flag-Gp8 using an anti-Flag antibody.

**b**, Representative plaque morphologies of WT or mutant T7 phages infecting WT *E. coli* MG1655 cells, imaged 18 h post infection.

427 **c**, Quantification of plaque sizes corresponding to panel **b** for WT and mutant T7 phages

428 infecting WT, Δ*relA*, or (p)ppGpp$^0$ (Δ*relA* Δ*spoT*) strains. Data are shown as scatter plots. **,

429 ***, and **** denote Student's *t*-test $P < 0.01$, 0.001, and 0.0001, respectively.

430 (**d**) Liquid infection assays of WT or mutant T7 phages infecting WT, Δ*relA*, or (p)ppGpp$^0$

431 (Δ*relA* Δ*spoT*) strains. Dashed lines indicate the time points at which 50% of the total

432 $OD_{600nm}$ decrease associated with lysis had occurred; corresponding durations and differences

433 are indicated.

434 **e**, Quantification of ATP, GTP, and (p)ppGpp levels in radiolabeled *E. coli* MG1655 cells

435 following infection with WT or mutant T7 phage. $OD_{600nm}$ values of the host cultures are

436 plotted on the secondary (right) *y*-axis. Experiments were performed in MOPS medium

437 supplemented with 0.2 mM $K_2HPO_4$ and 0.2% (w/v) glucose. Representative thin-layer

438 chromatography plates are shown in Supplementary **Fig. S7**. The first cycle of cell lysis

439 (indicated by a dashed line) occurred approximately 30 min post infection.

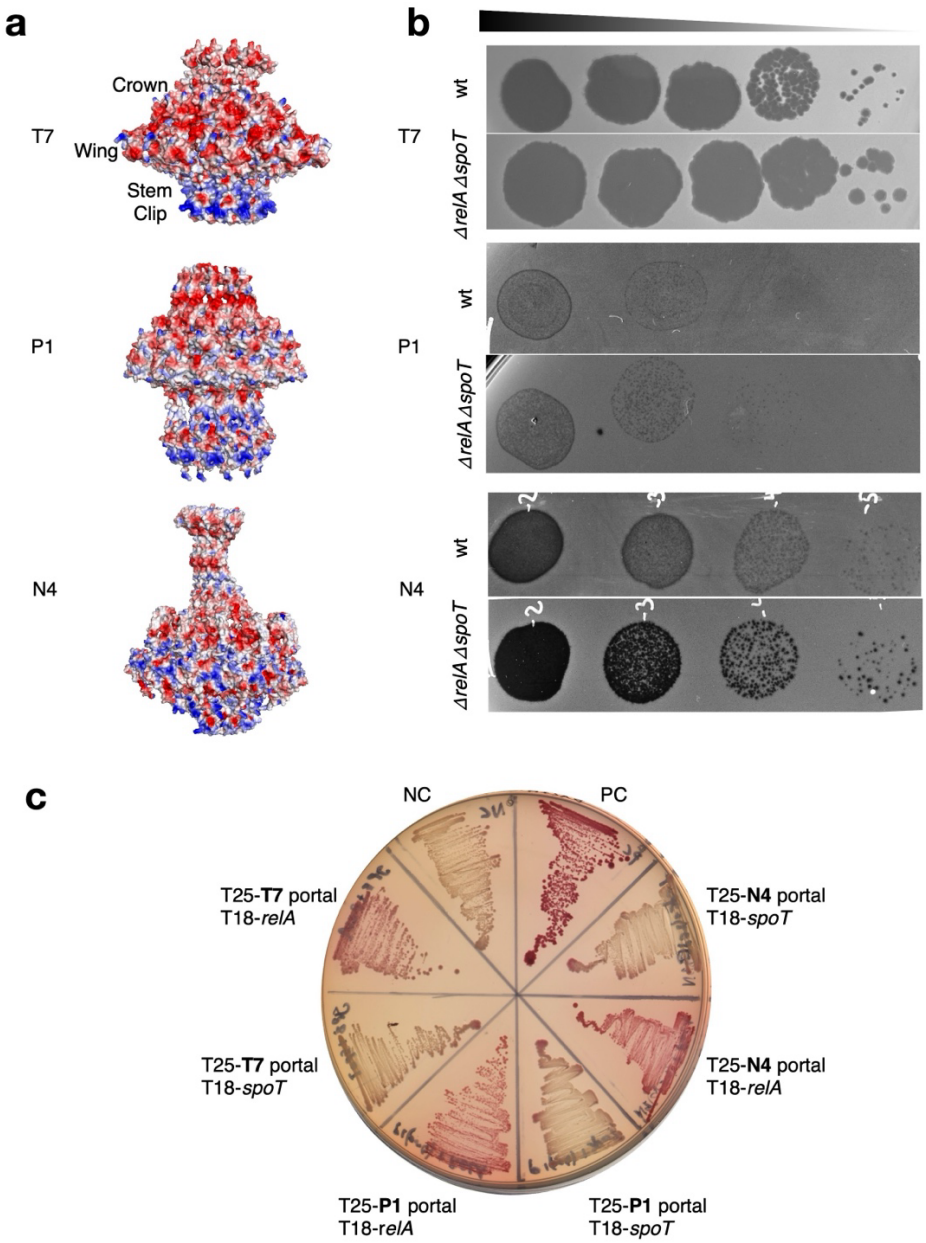


**Figure 6. Portal-mediated suppression of the stringent response is conserved among coliphages.**

**a**, Predicted structural models of portal proteins from representative coliphages (T7, P1, N4), colored by electrostatic surface potential, highlighting conserved charge patterning across portals. Due to computational limitations, only half of the portal ring is displayed.

**b**, Infection efficiency of representative phages assessed by tenfold serial dilution spotting on wild-type and (p)ppGpp$^0$ (*ΔrelA ΔspoT*) *E. coli* hosts.

448 **c**, Bacterial two-hybrid assays testing interactions between portal proteins from T7, P1, and

449 N4 and the alarmone synthetases RelA and SpoT, visualized on MacConkey indicator plates.

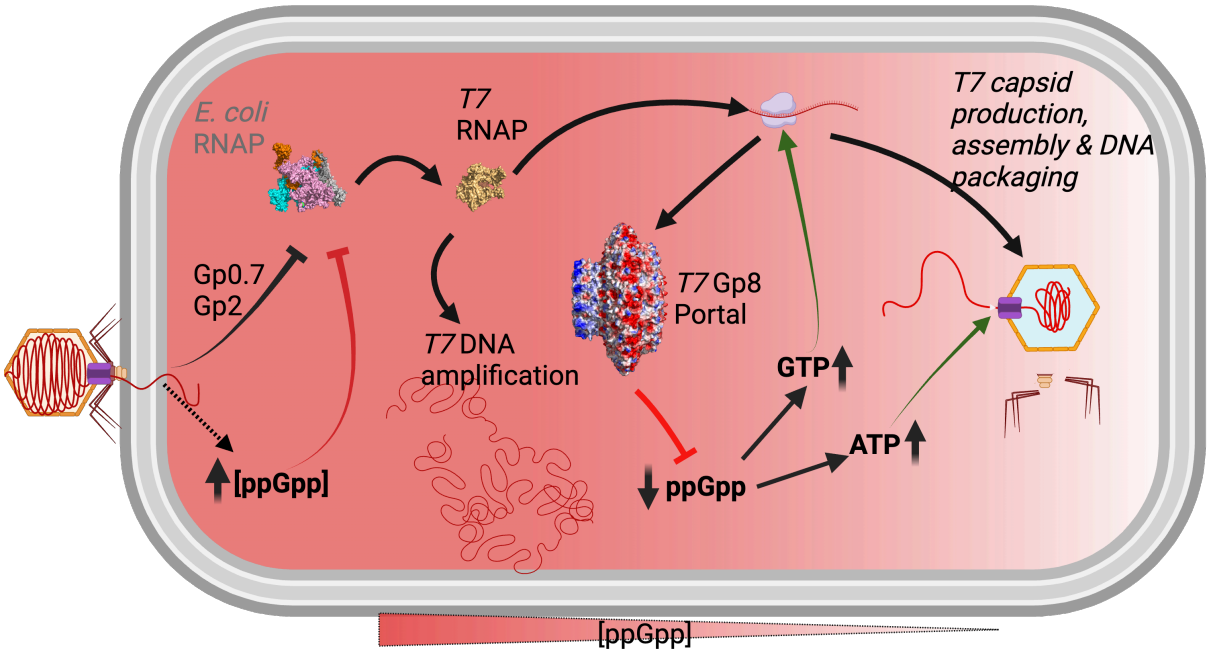


450

451 **Figure 7. Biphasic model for portal-mediated modulation of the stringent response**

452 **during phage infection.**

453 During early infection, phage entry and host takeover are associated with activation of the

454 stringent response and accumulation of (p)ppGpp, which suppresses host transcription and

455 contributes to the transition toward phage-directed gene expression. As infection progresses,

456 the structural portal protein Gp8 accumulates and engages the alarmone synthetases RelA and

457 SpoT, selectively inhibiting (p)ppGpp synthesis. Suppression of alarmone signaling restores

458 nucleotide availability and biosynthetic capacity required for late-stage viral protein

459 synthesis, genome packaging, and lysis. Portal-mediated targeting of stringent-response

460 enzymes is conserved among coliphages, indicating that modulation of alarmone signaling

461 represents a broadly conserved viral counter-defense strategy. (Created with BioRender.com)

462 **Supplementary figures**

463

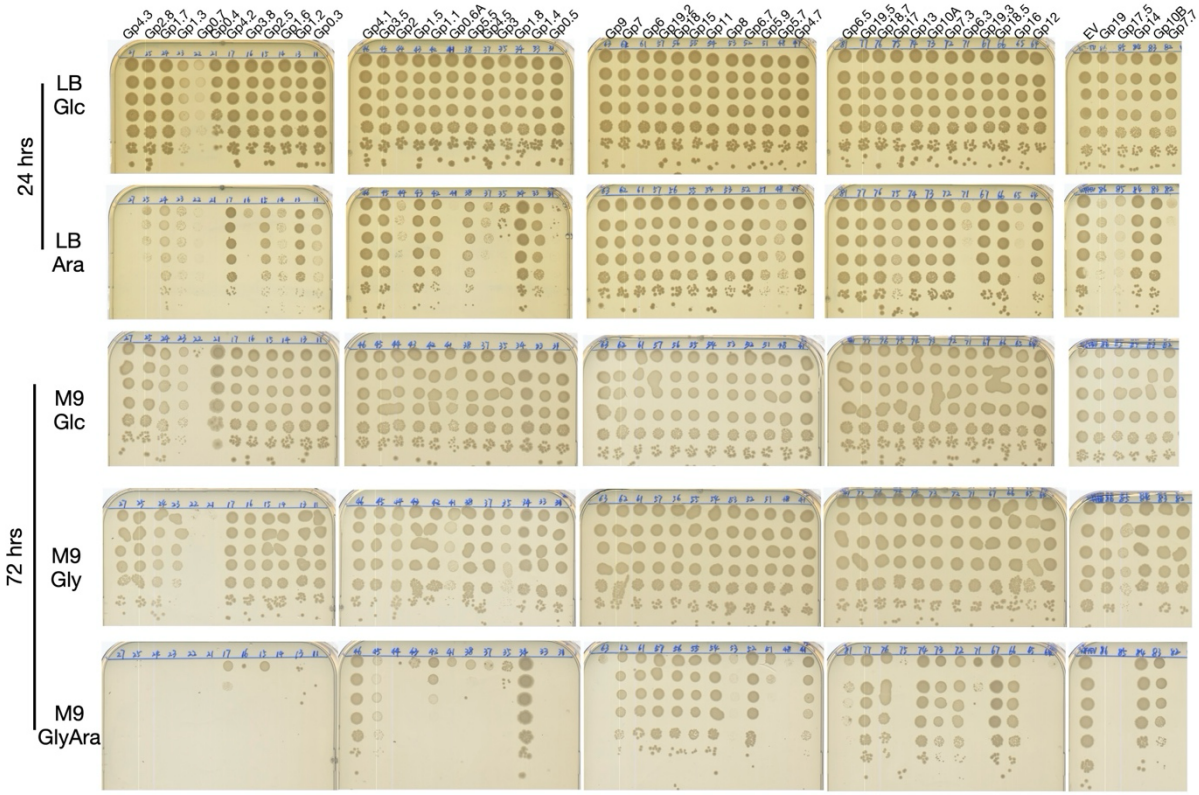


464

465 **Supplementary Fig. 1**

466 **Conditional toxicity of T7 proteins under nutrient limitation.**

467 Serial dilution assays showing growth of *Escherichia coli* expressing individual T7 genes in
468 rich and minimal media. Colony-forming units were normalized to $OD_{600nm}$. Expression of
469 multiple T7 proteins resulted in growth inhibition specifically under minimal-medium
470 conditions, whereas little or no effect was observed in rich medium. LB Glc and LB Ara are
471 LB media supplemented with 0.2% glucose and 0.2% arabinose, respectively. M9 Glc, M9 Gly,
472 and M9 Gly Ara denote M9 minimal media supplemented with 0.4% glucose, 0.4% glycerol,
473 or 0.4% glycerol plus 0.2% arabinose, respectively. LB plates were imaged after 24 h, and M9
474 plates after 72 h.

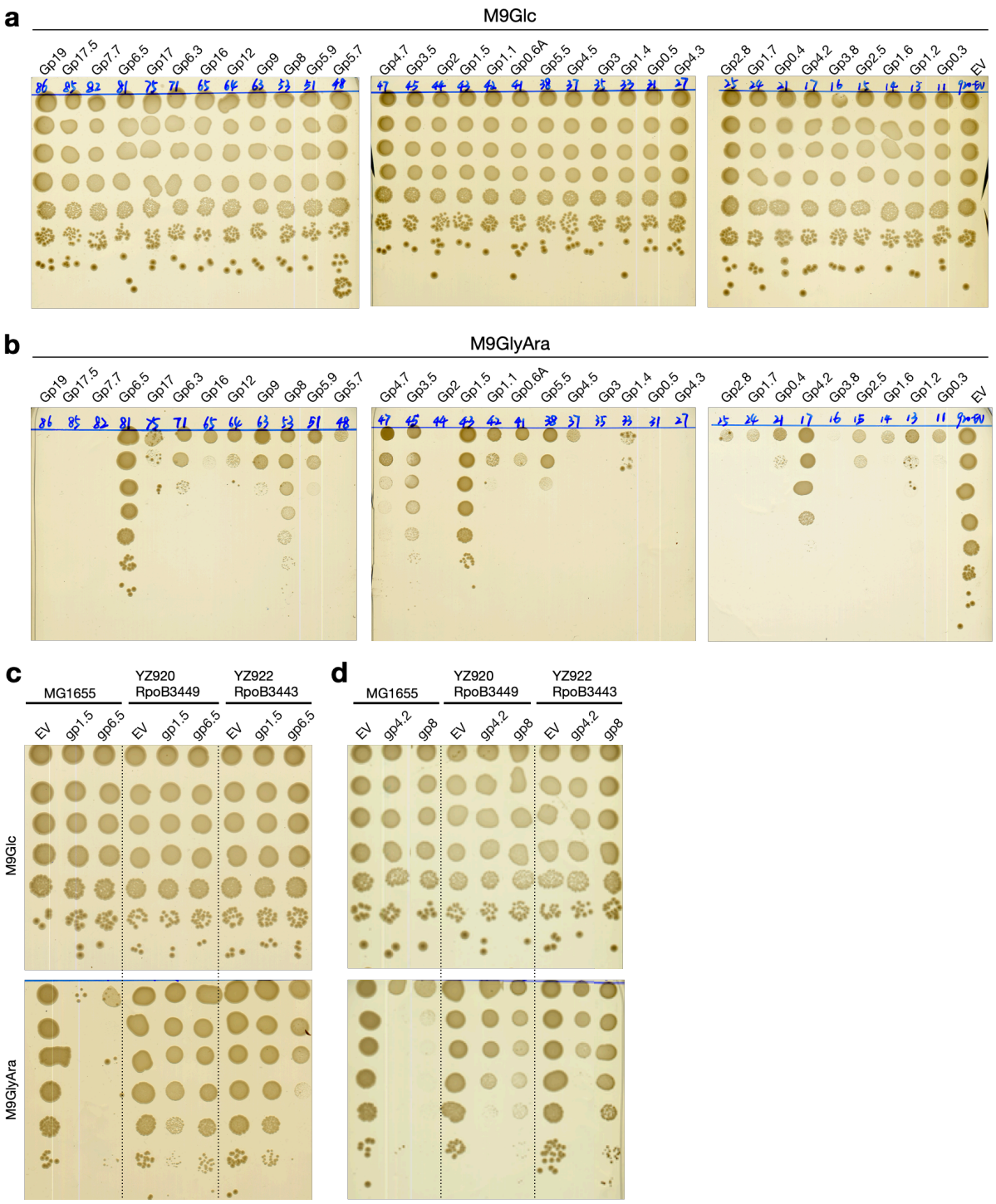


## Supplementary Fig. 2

**Suppression of T7 protein-induced growth defects by stringent-like RNA polymerase alleles.**

**a,b**, The YZ920 strain carrying the stringent-like *rpoB*3449 mutation was transformed with pBAD33 constructs expressing T7 proteins that were toxic in the wild-type *E. coli* MG1655

481 strain. Transformants were tested on M9 medium supplemented with glucose (M9Glc; **a**) or
482 glycerol plus arabinose (M9GlyAra; **b**) and incubated for 72 h.
483 **c,d**, Ten-fold serial dilutions (top to bottom) of wild-type MG1655 or YZ920 and YZ922
484 strains carrying the stringent-like *rpoB*3449 and *rpoB*3443 mutations, respectively, were
485 spotted onto M9Glc or M9GlyAra plates. Cells expressed the indicated T7 genes (*gp4.2*,
486 *gp1.5*, *gp8*, *gp6.5*) or an empty vector (EV). Plates were incubated at 37 °C and photographed
487 after 72 h.

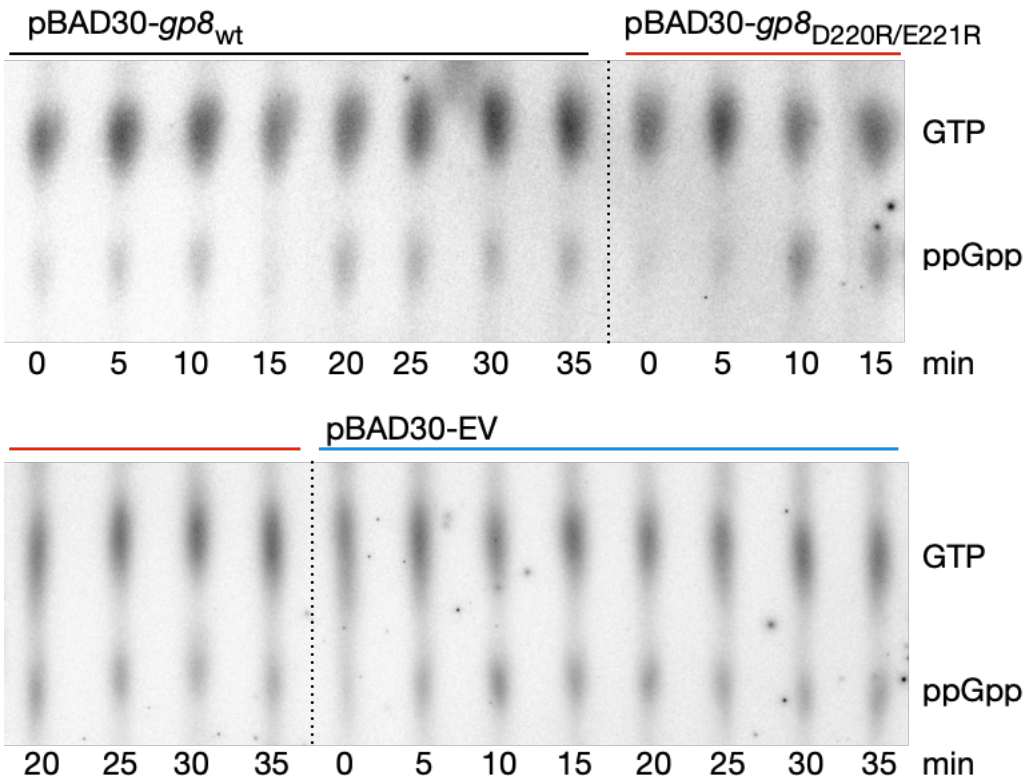

488

489 **Supplementary Fig. 3**

490 **Gp8 expression reduces intracellular (p)ppGpp accumulation.**
491 Thin-layer chromatography (TLC) analysis of **$^{32}$P**-labeled nucleotide pools during expression
492 of wild-type Gp8 or the interaction-defective mutant $Gp8_{D220R/E221R}$ from the pBAD30 vector.
493 Gp8 expression was induced with 0.2% arabinose, and 25 µL of each sample was analyzed

494 by TLC (see Materials and Methods for details). Positions of GTP and ppGpp are indicated,

495 along with the time points (minutes) following arabinose induction.

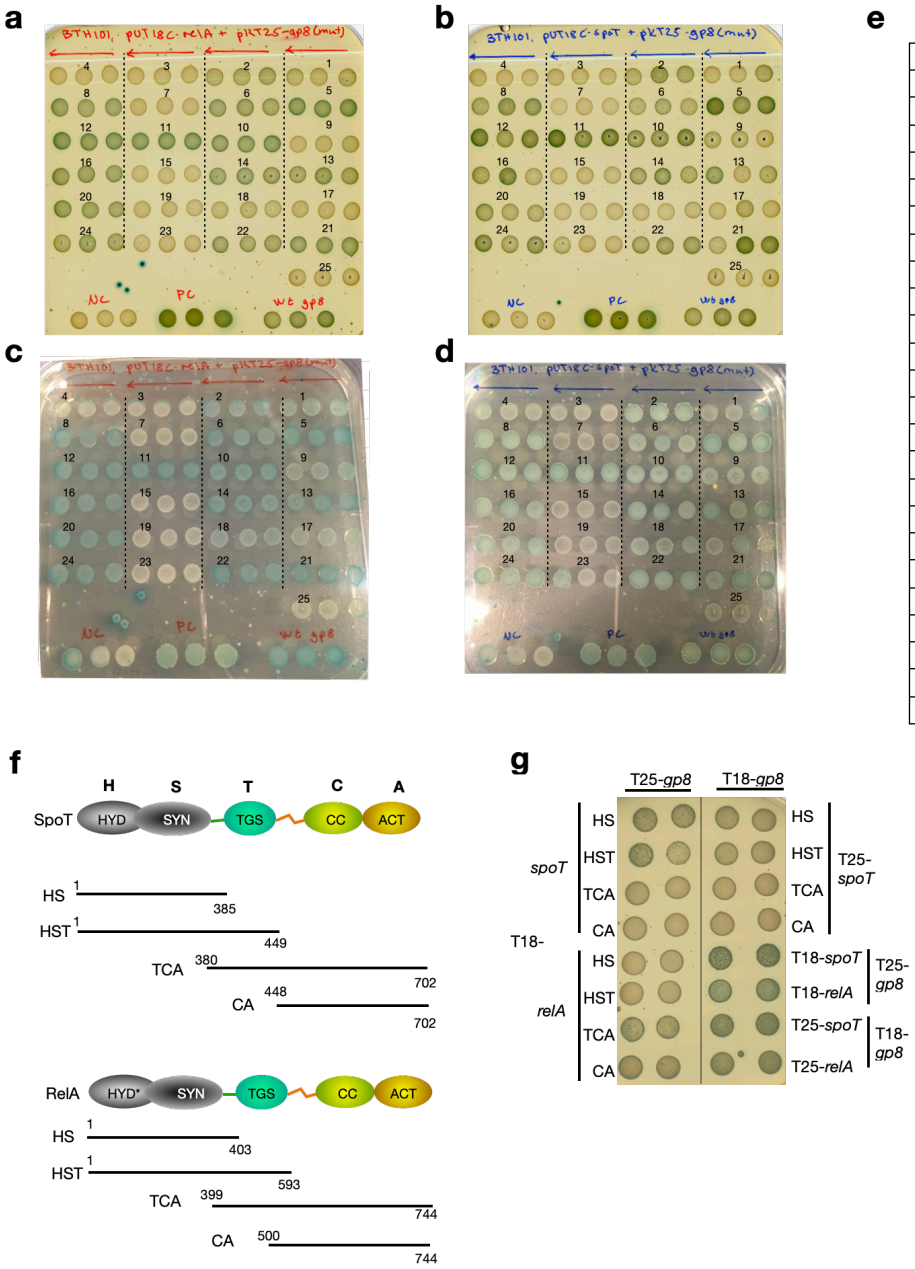


| | |
|---|---|
| 1 | *D46K/D48K/D53K* |
| 2 | D99K/D101K |
| 3 | D220R/E221R/D222R/E225R |
| **4** | **D220R/E221R** |
| 5 | D222R/E225R |
| 6 | D241K |
| 7 | **D457K/D460K** |
| 8 | D502R |
| 9 | *E10K/D11K* |
| 10 | E149K/E151K |
| 11 | E192R/D193K |
| 12 | E199R/E204R |
| 13 | E236R |
| 14 | E247R |
| **15** | **E280R/E284R** |
| 16 | E416K/E423K |
| 17 | *E485K/E486K* |
| 18 | *E521R/D528R* |
| 19 | **K4D/R5D** |
| 20 | K94D |
| 21 | K105E |
| 22 | K196E |
| 23 | **K288D/K295D** |
| 24 | K419D |
| 25 | *R277D* |

496

497 **Supplementary Fig. 4**

498 **Charge-reversal mutations in Gp8 disrupt interaction with RelA and SpoT.**

499 **(a-d)** Bacterial two-hybrid assays assessing interactions between charge-reversal mutants of

500 Gp8 and RelA **(a, c**; 24 h images**)** or SpoT **(b, d**; 48 h images**)**. Three independent replicate

spots are shown for each mutant. Mutations are numbered as indicated in panel **(e)**. Mutants shown in **bold** denote strongly defective interactions, whereas mutants shown in *italics* exhibit partial defects. **(f)**. Schematic overview of RelA and SpoT domain architectures and the truncation constructs tested in panel (**g**). Start and end residue numbers are indicated. (**g**) Bacterial two-hybrid assays assessing interactions between Gp8 and the RelA/SpoT truncations shown in (**f**). Two independent replicates are shown side by side.

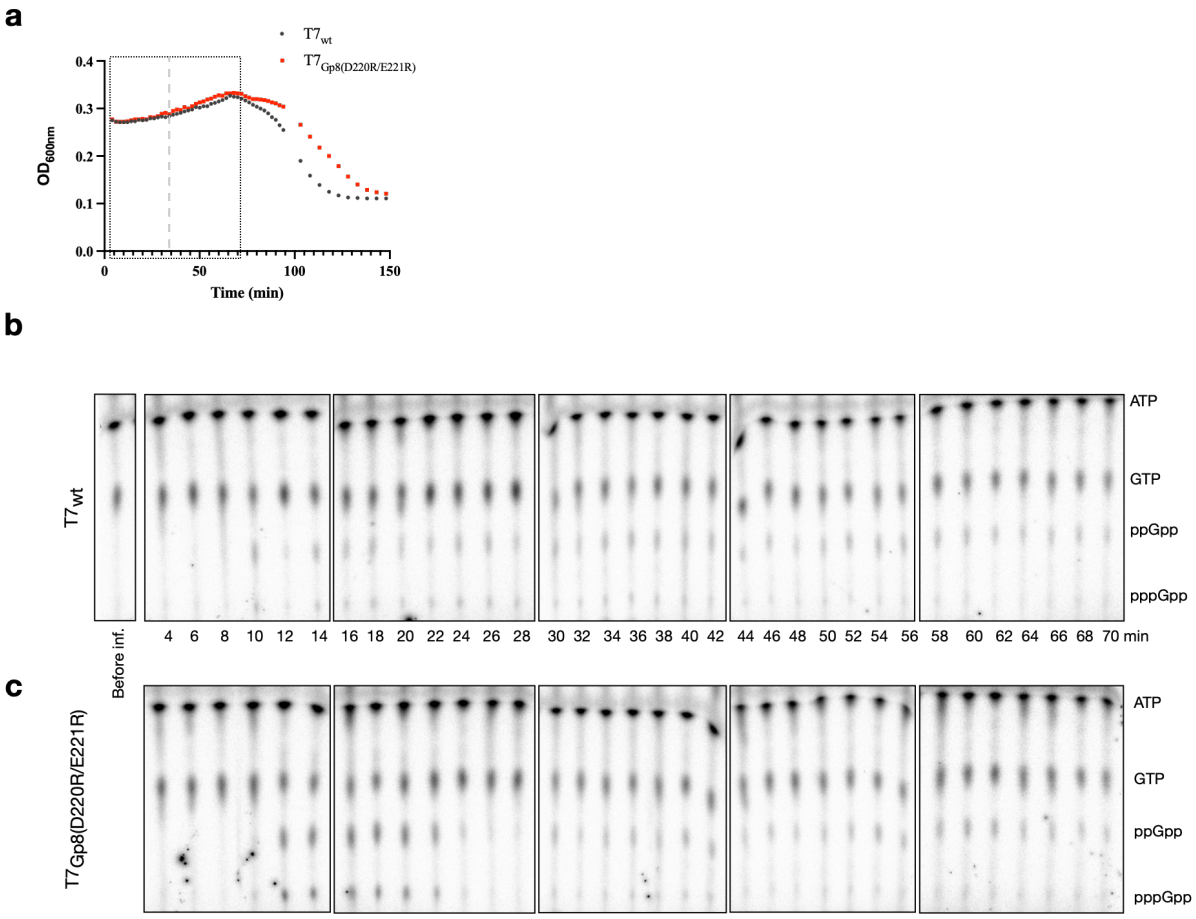


## Supplementary Fig. 5

**Sustained alarmone accumulation during infection with interaction-defective portal mutants.**

511 **(a)** Lysis kinetics of *E. coli* MG1655 growing in in MOPS minimal medium supplemented
512 with low phosphate (0.2 mM $K_2HPO_4$), and 0.2% (v/v) glucose, and infected with wild-type
513 T7 or gp8 interaction-defective mutant phages. The boxed region indicates the time window
514 quantified in **(b,c)** and shown in **Fig. 5e**.

515 **(b,c)** Radiolabeled nucleotide analysis of alarmone dynamics during phage infection.
516 Intracellular nucleotide pools were $^{32}$P-labeled during infection of *E. coli* MG1655 in MOPS
517 medium with T7 encoding wild-type gp8 **(b)** or interaction-defective gp8 **(c)**. The positions of
518 ATP, GTP, ppGpp, and pppGpp are indicated.

519

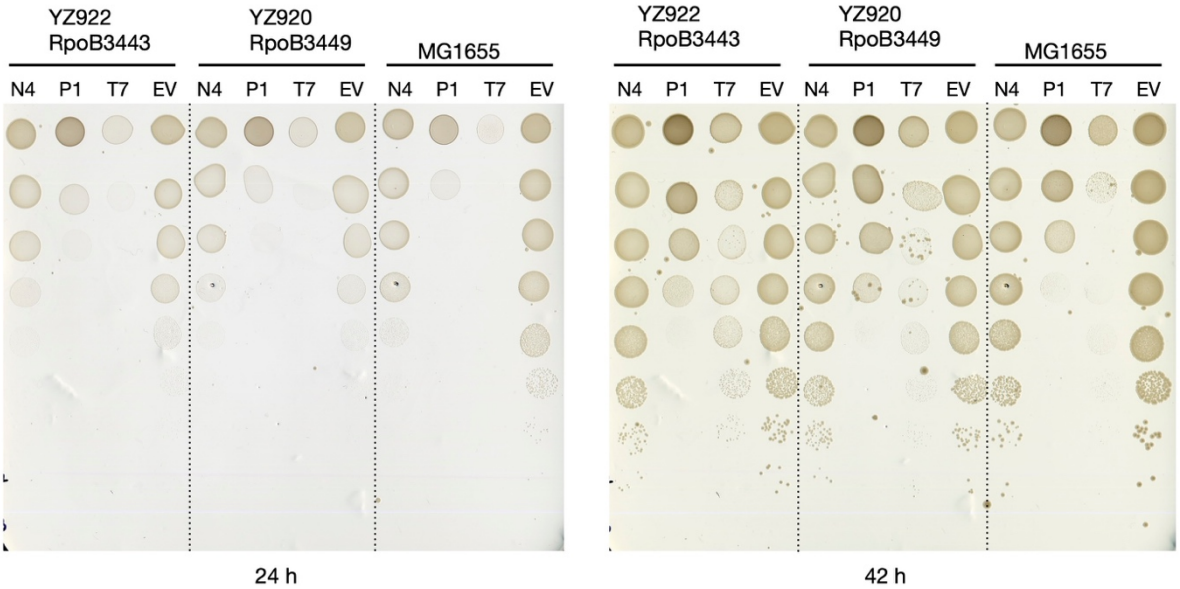


520

521 **Supplementary Fig. 6**

522 **Portal proteins from P1 and N4 exhibit stringent-response-linked phenotypes.**
523 Portal proteins from bacteriophages N4 and P1 were cloned into the arabinose-inducible
524 pBAD33 vector and expressed in wild-type *Escherichia coli* MG1655 or in stringent-response-
525 altered strains YZ920 and YZ922, carrying the *rpoB3449* and *rpoB3443* alleles, respectively.
526 Toxicity was assessed on M9 minimal medium supplemented with 0.4% glycerol and 0.2%

527 arabinose. Plates were imaged after 24 and 42 h of incubation at 37 °C. Labels N4, P1, and T7

528 denote portal proteins from the respective phages; EV indicates the empty-vector control.

529

530 ## Materials and Methods

531 **Bacterial strains and growth conditions**

532 All *Escherichia coli* strains and primers used in this study are listed in Supplementary
533 Document 1 and 3 respectively. Unless otherwise stated, *E. coli* K-12 MG1655 was used as the
534 wild-type background for infection assays and physiological analyses, and all derivative strains
535 were constructed in this background. *E. coli* DH5α was used for routine cloning, and *E. coli*
536 BL21(DE3) was used for protein expression. Bacteria were routinely grown in lysogeny broth
537 (LB) at 37 °C with aeration, with antibiotics added as required. For nucleotide labeling
538 experiments, cells were grown in defined MOPS minimal medium formulated with low
539 phosphate (0.2 mM $K_2HPO_4$), and 0.2% (v/v) glucose[36], to minimize background labeling from
540 inorganic phosphate. For experiments in defined nutrient conditions, cells were grown in M9
541 minimal medium supplemented with glucose (0.2% w/v), glycerol (0.4% v/v) as indicated.
542 Arabinose-inducible expression was achieved by addition of L-arabinose to a final
543 concentration of 0.2% (w/v). Growth and induction conditions are specified in the
544 corresponding figure legends.

545

546 **Phage strains and propagation**

547 Phages were propagated using *E. coli* MG1655 as host. A 50 mL MG1655 culture in LB
548 supplemented with 1 mM $MgCl_2$ and 1 mM $CaCl_2$ was grown at 37°C with shaking at 160 rpm
549 to an $OD_{600nm}$ of ~ 0.5. Phage stock (100 µL; PFU ~$10^8$-$10^{10}$) was added and incubation was
550 continued until extensive lysis was observed (1-3 h for T7). The lysate was treated with
551 chloroform (1 mL per 10 mL culture), vortexed, incubated for 5-10 min at room temperature,
552 and centrifuged (5 min, 5000 rpm). The supernatant was transferred to a new tube, centrifuged
553 again and collected into a clean tube. The phage stock was concentrated, and the buffer was
554 exchanged following the protocol described here[48]. Briefly, a 5× PEG solution (5 M NaCl, 20%

555 (w/v) PEG800) was added to the cleared lysate and incubated overnight at 4°C. The
556 precipitated phages were pelleted (1 h, 4°C, 19000 g), resuspended in 0.5-1 mL phage buffer
557 (150 mM NaCl, 40 mM Tris, 10 mM $MgSO_4$), and PFU was determined via plaque assay.
558 Phage stocks were stored at 4°C.
559
560 *Liquid killing assay*
561 *E. coli* strains MG1655, Δ*relA*, and Δ*relA*Δ*spoT*, were incubated overnight in LB medium at
562 37°C with shaking at 160 rpm. The following day, cultures were backdiluted into fresh LB
563 medium and incubated in flasks at 37°C with shaking at 160 rpm until reaching an $OD_{600nm}$ of
564 ~ 0.4. Cultures were normalized to $OD_{600nm}$=0.4, and 150 µL normalized culture was mixed
565 with T7 phage in a clear flat-bottom 96-well plate to the MOI=0.1. The $OD_{600nm}$ was recorded
566 via a plate reader (BioTek) every five minutes at 37°C without shaking.
567
568 *Plaque assay*
569 Plaque assays were performed as described here[49]. Briefly, cultures of the appropriate strains
570 were prepared in LB with appropriate antibiotics and incubated overnight at 37°C shaking at
571 160 rpm. The following day, cultures were adjusted to $OD_{600nm}$=2, and 200 µL normalized
572 culture was mixed with 100 µL of 10-fold serially diluted phage and incubated at room
573 temperature for 10 min. The mixtures were then mixed with 3 ml melted 0.7% LB agar (kept
574 at 50°C) and immediately poured onto prewarmed 1% LB agar plates. Plates were incubated
575 overnight at 37°C. For time-resolved plaque growth measurements, plates were imaged at
576 37 °C using the Reshape machine, and plaque diameter expansion over time was quantified
577 using ImageJ.
578
579 *T7 phage engineering*

580 To enable targeted mutagenesis of the essential T7 *gp8* gene, we established a genetic
581 dependency between the host and the phage based on the *trxA* gene, which is a host factor
582 essential for T7 replication. The endogenous *trxA* gene was deleted from the host chromosome,
583 rendering the host non-permissive to wild-type T7 infection. To restore infectivity, *trxA* was
584 introduced into the T7 genome via homologous recombination in place of *gp8*, and the *gp8* was
585 instead provided on the plasmid vector pCA24N[50] transformed to this Δ*trxA* host. This created
586 an interdependent system where the *gp8* sequence on the plasmid could be easily manipulated.
587 Due to homology sequences, the plasmid-encoded *gp8* mutant could integrate into its original
588 position on the T7 genome and thus create a mutant T7 particle that can be counter selected
589 using its independence of a plasmid borne *gp8*.
590
591 *Delete trxA in MG1655 using P1 phage transduction*
592 To delete *trxA* from *E. coli* MG1655, a P1 lysate was first prepared using *E. coli* Δ*trxA* strain
593 from the Keio collection[51]. Then, the P1 transduction method was used to generate a MG1655
594 Δ*trxA::kan* strain[52] and the kanamycin resistance maker was flipped out by using pCP20[53].
595
596 *Replace gp8 with trxA in T7*
597 The *trxA* gene was PCR-amplified using genomic DNA from *E. coli* strain MG1655 as a
598 template and primers pYZ1189 and pYZ1190, each containing 40 bp extensions homologous
599 to sequences flanking the *gp8* locus in the T7 phage genome. The purified PCR product was
600 introduced into *E. coli* MG1655 cells by electroporation during co-infection with T7 phage.
601 Immediately following electroporation, LB medium was added, and the culture was incubated
602 at 37°C,160 rpm until lysis was observed (around 1.5 hours). Phage lysates were then harvested
603 with chloroform and clarified via centrifugation (5 min, 5000 rpm).
604

605 *Cloning of pCA24N-gp8 and quick-change mutagenesis of gp8*

606 The *gp8* gene as well as 350 bp flanking regions from T7 was PCR amplified using primers
607 pYZ1191 and pYZ1192 that also encoded a *XhoI* and *HindIII* restriction site, respectively. This
608 PCR product as well as the pCA24N[50] plasmid were both digested with *XhoI* and *HindIII* and
609 ligated together using T4 ligase. The constructed pCA24N-gp8 was purified and used as
610 template for quick-change mutagenesis with primers pYZ1085-pYZ1136 (see Primer list).

611

612 *Constructing mutant T7 phages with gp8 mutations*

613 pCA24N plasmids encoding mutant *gp8* were purified and transformed into *E. coli* MG1655
614 Δ*trxA*. This strain was then infected with T7 *gp8::trxA* phage lysate (prepared as described
615 above). Through homologous recombination between the plasmid-encoded *gp8* mutant and
616 the corresponding flanking regions in the T7 genome (where *trxA* is inserted), the mutant *gp8*
617 sequence can replace *trxA*, and results in T7 progeny that carry the desired *gp8* mutation. The
618 mutant T7 phage particles can be counter selected using its independence of the pCA24N-
619 gp8.

620

621 **Measurement of (p)ppGpp by radiolabeling and autoradiography**

622 (p)ppGpp is a very labile molecule not suited for analysis by HPLC or mass spectrometry[54].
623 We therefore, performed thin layer chromatography (TLC) to quantify both pppGpp and ppGpp.
624 As phosphates in the medium impairs efficient incorporation of $H_3{}^{32}PO_4$ during labelling,
625 MOPS medium supplemented with low phosphate concentration (0.2 mM $K_2HPO_4$), and 0.2%
626 (v/v) glucose was used[36]. MG1655 was grown for ca. 18 hrs in MOPS-low$P_i$-Glc medium at
627 37 °C with agitation (160 rpm). Afterwards, the strains were adjusted to $OD_{600nm}$=0.05 in
628 MOPS-low$P_i$-Glc and grown at 37 °C with agitation (160 rpm) until $OD_{600nm}$ of 0.2-0-3 was
629 reached. Then, cells were transferred to a 2-ml Eppendorf tube and $H_3{}^{32}PO_4$ (equal to 100

630 μCi/ml) (Revvity, NEX053001MC) was added. After 1.5 h at 37 °C with 600 rpm agitation,
631 cells were transferred to a new tube and infected with T7 phage to an MOI of 0.1. Immediately
632 after, 150 μl infected cells were transferred to a clear 96-well plate and $OD_{600nm}$ at 37°C was
633 monitored every 2 min via a plate reader (BioTek). Simultaneously, 25 μl sample was collected
634 every 2 min and transferred to 5 μl cold 2 M formic acid. Samples were stores at -20°C until
635 analysed by TLC using 1.5 M $KH_2PO_4$ (pH 3.4) as mobile phase.
636
637 **Cloning all T7 genes into the pET28b and pBAD33 vectors**
638 Genomic DNA of *E. coli* T7 bacteriophage was used as the template for amplification of
639 individual T7 genes with Q5 High-Fidelity DNA polymerase (New England Biolabs). PCR
640 amplicons were gel-purified, quantified spectrophotometrically, and digested with *EcoRI* and
641 *NcoI* at 37°C for 3 h followed by enzyme inactivation at 80°C for 20 min. The digested
642 fragments were ligated into the similarly treated pET28b vector using T4 DNA ligase at room
643 temperature for 30 min. Ligation mixtures were transformed into chemically competent *E. coli*
644 DH5α cells and plated on LB agar supplemented with kanamycin (25 μg $mL^{-1}$). Individual
645 transformants were screened by colony PCR, and clones displaying expected insert sizes were
646 cultured in LB medium for plasmid purification. All constructs were verified by Sanger
647 sequencing, yielding a pET28b-T7 gene library encompassing 51 of 59 targeted genes; 8 highly
648 toxic genes could not be cloned or yielded unstable plasmids.
649
650 To place the T7 genes under the arabinose-inducible promoter, verified pET-T7 plasmids were
651 digested with *XbaI*, *HindIII* and *EcoRV*, and ligated into pBAD33 linearized with *XbaI* and
652 *HindIII*. This procedure transferred the pET Shine-Dalgarno sequence and corresponding T7
653 gene inserts into pBAD33 under the control of the pBAD promoter. Using the iVEC cloning
654 strategy[55], we successfully obtained pBAD33-*gp0.4* and pBAD33-*gp0.7* plasmids, the pET

655 versions of which were impossible. The resulting library, designated pBAD-T7, comprised 53
656 T7 genes. For expression of T7 proteins in strain YZ921, the T7 genes were subcloned from
657 the pBAD33 (cat) vector into the pBAD30 (bla) vector using the *XbaI* and *HindIII* restriction
658 sites, as YZ921 carries a chloramphenicol resistance gene (cat).
659

660 **Toxicity assay of pBAD33-T7 genes on five media**

661 Each of the 53 verified pBAD-T7 plasmids was individually transformed into chemically
662 competent *E. coli* MG1655 cells. Transformants were streaked as single colonies on LB agar
663 plates supplemented with chloramphenicol (25 μg $mL^{-1}$) and a single colony from each
664 transformant was inoculated into 1 mL LB broth and cultured overnight at 37°C with shaking
665 (200 rpm). From each culture, 300 μL was diluted in 800 μL fresh LB to measure optical
666 density at 600 nm ($OD_{600nm}$), while another 300 μL aliquot was pelleted by centrifugation at
667 13,000 rpm for 3 min, washed twice with 1 mL PBS, and resuspended to an $OD_{600nm}$ = 1. Serial
668 tenfold dilutions ($10^8$-$10^1$ CFU $mL^{-1}$) were prepared in 96-well plates by mixing 20 μL of
669 bacterial suspension with 180 μL PBS per well. From each dilution, 5 μL was spotted onto five
670 pre-dried chloramphenicol-containing agar media: LB + 0.4% glucose, LB + 0.2% L-arabinose,
671 M9 + 0.4% glucose, M9 + 0.4% glycerol, and M9 + 0.4% glycerol + 0.2% L-arabinose. Plates
672 were incubated at 37°C and photographed every 24 h to monitor colony growth and induction-
673 dependent phenotypic changes.
674

675 **Construction of bacterial two-hybrid vectors**

676 <u>*Cloning relA, spoT and their truncates*</u>

677 *spoT* and *relA* were cloned into the bacterial two-hybrid vectors pUT18C and pKT25. The
678 full-length genes were amplified from *E. coli* MG1655 chromosomal DNA using primer pairs
679 pYZ479/pYZ480 (*spoT*) and pYZ481/pYZ482 (*relA*). PCR products and recipient plasmids

680 were digested with *XbaI* and *XmaI*, ligated, and transformed into *E. coli*. Truncated *spoT*
681 variants corresponding to the HS, HST, TCA, and CA regions were generated by PCR using
682 primer pairs pYZ473/pYZ474, pYZ473/pYZ475, pYZ477/pYZ476, and pYZ478/pYZ476,
683 respectively. The resulting fragments were digested with *XbaI*/*XmaI* and cloned into pUT18C
684 or pKT25. Truncated *relA* variants (HS, HST, TCA, and CA) were amplified using primer
685 pairs pYZ917/pYZ919, pYZ917/pYZ918, pYZ920/pYZ921, and pYZ920/pYZ922,
686 respectively, digested with *XbaI*/*XmaI*, and cloned into pUT18C.

687 *Cloning of the portal protein from phages P1 and N4 into pKT25*
688 Portal protein from phages P1 and N4 were amplified using primer pairs pYZ1285/pYZ1286
689 and pYZ1287/pYZ1288 for phage P1 and N4, respectively. The pKT25 was digested with *KpnI*
690 and *EcoRI*, assembled with both PCR products by the iVEC cloning method[55].
691 *pUT18-rpoZ and pKNT25-rpoZ*
692 To generate pUT18-*rpoZ*, the full-length *rpoZ* gene was PCR-amplified from *E. coli* MG1655
693 genomic DNA using primers pYZ867 and pYZ868. The amplified fragment and pUT18 vector
694 were digested with *HindIII* and *XbaI*, ligated, and transformed into *E. coli* DH5α. For
695 construction of pKNT25-*rpoZ*, the pKNT25 vector was first modified by site-directed
696 mutagenesis using primers pYZ871 and pYZ872 following the QuickChange protocol to
697 introduce an *NcoI* restriction site, generating pKNT25-*NcoI*. The *rpoZ* insert was excised from
698 pUT18-rpoZ by digestion with *ScaI*, *HindIII*, and *XbaI*, and ligated into *HindIII*/*XbaI*-digested
699 pKNT25-*NcoI*.

700 *pUT18/KT25-gp4.2/gp1.5/gp8/gp6.5*

701 An *NcoI* restriction site was introduced into pUT18C (YZ709) by site-directed mutagenesis
702 using primers pYZ864 and pYZ866, generating pUT18C-*NcoI*. For pKT25 (YZ705), the
703 native *NcoI* site was first removed using primers pYZ863 and pYZ862, followed by

704 introduction of a new *NcoI* site using primers pYZ864 and pYZ865 to generate pKT25-*NcoI*.
705 Plasmids pET28-gp4.2, pET28-gp1.5, pET28-gp8, and pET28-gp6.5 were digested with
706 *EcoRI*, *NcoI*, and *HindIII*, and the resulting inserts were individually cloned into pUT18C-
707 *NcoI* or pKT25-*NcoI* vectors digested with *NcoI* and *HindIII*.

708 *Construction of Gp8 truncations*

709 Truncations of Gp8 were generated by site-directed mutagenesis of the *gp8* gene on the pKT25
710 vector in *E. coli* DH5a using the QuickChange method. Primer pairs pYZ1063/pYZ1064,
711 pYZ1065/pYZ1066, pYZ1067/pYZ1068, and pYZ1069/pYZ1070, were used to construct the
712 clip truncation, clip+stem truncation, N-terminal truncation, and C-terminal truncation,
713 respectively. PCR reactions were carried out with Q5 DNA polymerase using an extension
714 time of 3 min and an annealing temperature gradient of 50-70°C across eight 12 µL samples.
715 After amplification, the samples were pooled and digested with 2.5 µL *DpnI* at 37°C for 3 h,
716 followed by inactivation at 80°C for 20 min. The reaction mixture was then transformed into
717 *E. coli* DH5a via chemical transformation. Successful truncations were confirmed by Sanger
718 sequencing using primers pYZ471 and pYZ472.
719

720 **Bacterial two-hybrid assay**

721 The bacterial two-hybrid assay was performed using *Escherichia coli* strain BTH101. Cells
722 were co-transformed with plasmids pUT18C and pKT25, with one plasmid encoding either
723 *relA* or *spoT* and the other encoding the phage gene of interest. Transformants were selected
724 on LB agar supplemented with 0.2% (w/v) glucose, 25 µg $mL^{-1}$ kanamycin, and 100 µg $mL^{-1}$
725 ampicillin and incubated at 37 °C. Single colonies were used to inoculate overnight cultures
726 grown at 37 °C with shaking at 170 rpm. The following day, cultures were washed twice with
727 phosphate-buffered saline (PBS) and resuspended in PBS to a final optical density of $OD_{600nm}$

728 = 5. Aliquots (5 µL) of the normalized cell suspensions were spotted onto LB agar containing
729 25 µg $mL^{-1}$ kanamycin, 100 µg $mL^{-1}$ ampicillin, and 40 µg $mL^{-1}$ X-gal. Plates were incubated
730 at 30 °C overnight. Plates were scanned, and spot intensities were quantified using ImageJ.
731 Images were converted to RGB stacks, the red channel was isolated and inverted, and the mean
732 intensity of each spot was measured. Background signal from negative controls was subtracted
733 from all samples. Interaction strengths were normalized and expressed as a percentage of the
734 positive control or full-length protein interaction, as specified in the figure legends.
735
736
737 **Cloning of the pET28-HMS-relA and -spoT vectors**
738 *pET28-HMS-spoT* and derivatives
739 Plasmids pET28a and pMAL-c2x were digested with *NdeI* and *EcoRI* and ligated to generate
740 pET28-$His_6$-MBP (YZ913). The *sumo* and *spoT* genes were PCR-amplified using primers
741 pYZ692/693 and pYZ694/695, fused by overlap PCR, and cloned into pET28a using *NcoI* and
742 *HindIII* to generate pET28a-$His_6$-SUMO-SpoT (YZ307). The SUMO-SpoT fragment was
743 excised with *EcoRI* and *HindIII* and ligated into pET28a-$His_6$-MBP. Missing SUMO sequences
744 were amplified using primers pYZ684/685, digested with *EcoRI*, and inserted into this
745 intermediate construct to generate pET28-$His_6$-MBP-SUMO-SpoT (pET28-HMS-spoT).
746
747 *Generation of SpoT point mutants*
748 The E319Q and H72A/D73A mutations were introduced into pET28-HMS-spoT using PCR-
749 amplified fragments derived from chromosomal *spoT* mutant strains YZ586 and YZ905,
750 respectively[56]. PCR products generated with primers pYZ702 and pYZ703 were digested with
751 *PmlI* and *SalI* and ligated into pET28-HMS-spoT to generate the corresponding mutant

752 constructs. The *spoT* gene was deleted from pET28-HMS-spoT using primers pYZ905 and
753 pYZ906 to generate the pET28b-HMS vector (YZ1515).
754
755 Construction of *pET28-HMS-relA*
756 The *relA* gene was PCR-amplified from *E. coli* MG1655 using primers pYZ927 and pYZ928.
757 Both the PCR product and pET28b-HMS were digested with *BamHI* and *HindIII*, ligated using
758 T4 DNA ligase, and transformed into *E. coli* DH5α to generate pET28-HMS-relA.
759
760 **Pull down and Western blot**
761 Overnight cultures of *E. coli* BL21 DE3 strains expressing pRARE, pET28b-HMS, -*relA* or -
762 *spoT*, and pBAD30-*gp8-Flag* (see Strain list) were incubated in LB medium with 25 µg/mL
763 kanamycin, 25 µg/mL chloramphenicol, and 30 µg/mL ampicillin at 37°C with shaking at 160
764 rpm. The following day, cultures were back-diluted to an $OD_{600nm}$ of 0.05 in 50 mL fresh LB
765 medium containing the same antibiotics as above and incubated at 37°C with shaking at 160
766 rpm until reaching $OD_{600nm}$ of ~ 0.2-0.3. Gene expression was induced by addition of arabinose
767 and IPTG to final concentrations of 0.2% and 0.5 mM, respectively, followed by incubation
768 for 4 hours at 37°C with shaking at 160 rpm. Cells were harvested by centrifugation (10 min,
769 4000 rpm, 4°C), resuspended in 10 mL PBS and centrifuged again as above. Supernatant was
770 discarded and cell pellets were stored at -20°C. Pellets were thawed on ice, resuspended in 400
771 µL lysis buffer (50 mM HEPES (pH 8), 0.25 M NaCl, 10 mM imidazole, 200 µM $ZnCl_2$, and
772 2 mM $MgCl_2$) and disrupted with glass beads (Sigma, G4649) using a MagNA Lyser (20 s at
773 6500 rpm, done twice with cooling on ice between runs). Lysates were centrifuged (5 min,
774 5000 rpm, 4°C) and supernatants were collected. Total protein concentration was measured via
775 Bradford Assay, and samples were normalized with lysis buffer to equal total protein
776 concentrations. Equal volumes of normalized lysates were incubated with 50 µL Ni-NTA

777 Agarose resins (Qiagen) overnight at 4°C with gentle inversion. The next day, samples were
778 centrifuged (2 min, 1000 rpm, 4°C), and supernatant was removed. Resins were gently
779 resuspended with 1 mL lysis buffer and incubated for 1 h at 4°C with gentle inversion. Samples
780 were centrifuged (2 min, 1000 rpm, 4°C), and supernatant was removed. Resins were
781 subsequently resuspended in 1 mL wash buffer (50 mM HEPES (pH 8), 0.25 M NaCl, 20 mM
782 imidazole, 200 µM $ZnCl_2$, 2 mM $MgCl_2$) and incubated for 1 h at 4°C with gentle inversion.
783 Following incubation, samples were transferred to a 0.5 mL Eppendorf tube and centrifuged
784 (first for 2 min at 1000 rpm, then for 1 min at 13000 rpm). Supernatant was removed and
785 proteins were eluted with 20 µL elution buffer (50 mM HEPES (pH 8), 0.25 M NaCl, 1.25 M
786 imidazole, 200 µM $ZnCl_2$, 2 mM $MgCl_2$) to yield a final imidazole concentration of
787 approximately 500 mM). Samples were incubated for 15 min at 4°C (gently disturbing the
788 resins occasionally). Samples were then centrifuged (2 min, 1000 rpm), and 35 µL supernatant
789 was transferred to 11.6 µL 4x Leammli buffer, boiled for 15 min at 95°C and 12 µL of each
790 sample was loaded onto a 10% SDS-PAGE gel. Following electrophoresis, proteins were
791 transferred to a PVDF membrane by wet transfer (300 mA, 1 h, 4°C) using transfer buffer
792 composed of 20% methanol, 0.2 M glycine, and 25 mM Tris (pH 8.3). Membrane was blocked
793 overnight at 4°C in TBST + 5% (w/v) milk powder. Next day, the membrane was incubated
794 with anti-FLAG primary antibody diluted in TBST + 5% (w/v) milk powder for 1 h, 4°C,
795 washed three times (10 min each) in TBST, and subsequently incubated with anti-mouse
796 secondary antibody in TBST + 5% (w/v) milk powder for 1 h, 4°C. After three additional
797 washes in TBST, the membrane was developed using Pierce® ECL Western Blotting Substrate
798 (Thermo Scientific, #32209) and imaged via ImageQuant LAS4000.
799
800 **Protein purification for biochemical assays**

801 RelA (YZ1607), SpoT hydrolysis only (HYD, YZ1063), SpoT synthesis only (SYN, YZ1070),
802 and Gp8 (YZ1632) constructs bearing an N-terminal His-MBP-SUMO (HMS) tag were
803 expressed from pET28b in *E. coli* BL21(DE3). Overnight cultures of these strains were grown
804 in LB medium supplemented with appropriate antibiotics at 37°C, with shaking at 160 rpm.
805 The following day, cultures were back-diluted 1:50 into 0.5 L fresh LB medium supplemented
806 with appropriate antibiotics and grown at 37°C with shaking at 160 rpm until reaching an OD
807 of 0.4-0.7. Protein expression was induced by the addition of IPTG to a final concentration of
808 0.1 mM, and cultures were incubated overnight at 24°C, shaking with aeration. The next day,
809 cells were harvested by centrifugation (5000 rpm, 10 min, 4°C), washed in 30 mL cold PBS,
810 and pelleted again (4000 rpm, 20 min, 4°C). Resulting pellets were resuspended in 40 mL cold
811 lysis buffer (50 mM Tris-HCl pH=8, 1 M NaCl, 2 mM DTT, 10 mM imidazole) supplemented
812 with Pierce™ Protease Inhibitor Mini (Thermo Scientific, A32955). Cells were lysed by
813 sonication on ice for 24 min at 20% amplitude, and lysates were cleared by centrifugation
814 (14000 rpm for 45 min at 4 °C). Cleared lysates were incubated with 0.5-1 mL Ni-NTA
815 Agarose resins (Qiagen) overnight at 4°C with gentle inversion. The next day, the resins were
816 collected by centrifugation (1000 rpm, 2 min) and washed once with 30 mL lysis buffer (1 h,
817 4°C), followed by 30 mL wash buffer (same composition as lysis buffer, except imidazole
818 increased to 20 mM). Resins were transferred onto a Bio-Rad Gravity Flow Column, and bound
819 proteins were eluted with 700 µL elution buffer (50 mM tris-HCl pH=8, 1 M NaCl, 2 mM DTT,
820 500 mM imidazole). The eluted fraction was subjected to size-exclusion chromatography using
821 an ÄKTA Pure™ system (Cytiva) equilibrated gel filtration buffer (50 mM HEPES pH=8, 1
822 M NaCl, 2 mM DTT, 5% glycerol). Protein concentrations were determined via Bradford
823 Assay.
824
825 **Synthesis of [α-$^{32}$P](p)ppGpp via RelSeq**

826 [α-$^{32}$P](p)ppGpp was synthesized using[α-$^{32}$P]GTP (revvity, BLU006X250UC) as substrate in
827 a RelSeq-catalyzed reaction[57]. RelSeq (YZ8) was expressed and purified as described above
828 except that protein expression was induced with 0.5 mM IPTG for 3 h at 30°C. The purification
829 buffer contained 500 mM NaCl, 50 mM Tris-HCl (pH 8), and 5% glycerol, with imidazole
830 concentrations of 20, 40, and 500 mM for lysis, wash, and elution buffers, respectively. The
831 gel filtration buffer was identical but without imidazole. For the enzyme reaction, a 10×
832 reaction buffer was prepared containing 250 mM Tris (pH 9), 1 M NaCl, and 150 mM $MgCl_2$.
833 The final reaction system contained 1× reaction buffer, 8 mM ATP, 125 nM [α-$^{32}$P]GTP, and
834 4 μM RelSeq, and was incubated at 37°C for 1 h. The reaction was terminated by boiling for 5
835 min at 95°C, followed by centrifugation (14000 rpm, 5 min). Conversion of substrate was
836 verified by thin-layer chromatography (TLC) using 0.5 μL of the reaction mixture and 1.5 M
837 $KH_2PO_4$ (pH 3.4) as the mobile phase.
838
839 **Biochemical assays**
840 Synthetase activity of RelA and SpoT (SYN), was assayed in reaction mixtures containing 50
841 mM HEPES (pH 7.4), 100 mM KCl, 5 mM $MgCl_2$, 2 mM DTT, 0.2 mg/mL BSA, 2 mM GTP,
842 and 6 nM [α-$^{32}$P] GTP (revvity, BLU006X250UC) were prepared. Protein was added to final
843 concentrations of 0.5 μM (RelA) or 3 μM (SpoT (SYN)). Gp8 was added to varying final
844 concentrations, and samples were incubated at room temperature for 10 min before enzyme
845 reactions were initiated by addition of 5 mM ATP. Hydrolase activity of SpoT (HYD) was
846 assayed in a reaction mixture containing 50 mM HEPES (pH 8), 100 mM KCl, 5 mM $MnCl_2$,
847 2 mM DTT, and 0.2mg/mL BSA was prepared. SpoT (HYD) was added to a final concentration
848 of 100 nM, while Gp8 was added at varying final concentrations. Reaction mixtures were
849 incubated at room temperature for 10 min before enzyme reaction was initiated by the
850 simultaneous addition of cold ppGpp (Jena Biocience, NU-884L), and hot [α-$^{32}$P](p)ppGpp to

851 final concentrations of 31.25 and 6 nM, respectively. Enzyme reactions were stopped by
852 transferring 4 µL of the reaction mixtures into 1 µL cold 250 mM EDTA (final concentration
853 50 mM). Samples were loaded onto a PEI Cellulose plates and resolved using 1.5 M $KH_2PO_4$
854 (pH 3.4) as the mobile phase. Plates were exposed to a BAS-MS imaging plate and scanned
855 using a Typhoon phosphorimager.
856

857 **Acknowledgements**

858 We would like to thank Jeppe Aaby Andersen for cloning of the portal protein from phages P1
859 and N4 into the bacterial two-hybrid system, and for testing their interaction with RelA and
860 SpoT. We would also like to thank Sonia de Araujo and Anette Vestergaard for cloning of the
861 *relA*, *spoT* and their truncates into the bacterial two-hybrid system. We thank Yueyue Liu for
862 preparing stocks of the selected phages obtained from the BASEL Collection. We are grateful
863 for Michael J Gray's gifting of the $RNAP^{SR}$ strains. The work is supported by a Danmarks Frie
864 Forskningsfond grant (2032-00030B) and the Carlsberg Foundation Semper Ardens Accelerate
865 grant (CF24-1843) to Y.E.Z. and the Chinese Scholarship Council program (202006330098)
866 to L.K.W.

867 **References**


868 1 Egido, J. E., Costa, A. R., Aparicio-Maldonado, C., Haas, P. J. & Brouns, S. J. J.
869 Mechanisms and clinical importance of bacteriophage resistance. *FEMS Microbiol*
870 *Rev* **46** (2022). https://doi.org/10.1093/femsre/fuab048
871 2 Georjon, H. & Bernheim, A. The highly diverse antiphage defence systems of
872 bacteria. *Nat Rev Microbiol* **21**, 686-700 (2023). https://doi.org/10.1038/s41579-
873 023-00934-x
874 3 Hochhauser, D. & Sorek, R. Manipulation of the nucleotide pool in human, bacterial
875 and plant immunity. *Nat Rev Immunol* **26**, 7-22 (2026).
876 https://doi.org/10.1038/s41577-025-01206-w
877 4 Bernheim, A. & Sorek, R. The pan-immune system of bacteria: antiviral defence as a
878 community resource. *Nat Rev Microbiol* **18**, 113-119 (2020).
879 https://doi.org/10.1038/s41579-019-0278-2
880 5 Lopatina, A., Tal, N. & Sorek, R. Abortive Infection: Bacterial Suicide as an Antiviral
881 Immune Strategy. *Annu Rev Virol* **7**, 371-384 (2020).
882 https://doi.org/10.1146/annurev-virology-011620-040628
883 6 Potrykus, K. & Cashel, M. (p)ppGpp: still magical? *Annual review of microbiology* **62**,
884 35-51 (2008). https://doi.org/10.1146/annurev.micro.62.081307.162903
885 7 Irving, S. E., Choudhury, N. R. & Corrigan, R. M. The stringent response and
886 physiological roles of (pp)pGpp in bacteria. *Nat Rev Microbiol* **19**, 256-271 (2021).
887 https://doi.org/10.1038/s41579-020-00470-y
888 8 Hauryliuk, V., Atkinson, G. C., Murakami, K. S., Tenson, T. & Gerdes, K. Recent
889 functional insights into the role of (p)ppGpp in bacterial physiology. *Nat Rev*
890 *Microbiol* **13**, 298-309 (2015). https://doi.org/10.1038/nrmicro3448
891 9 Nowicki, D., Kobiela, W., Wegrzyn, A., Wegrzyn, G. & Szalewska-Palasz, A. ppGpp-
892 dependent negative control of DNA replication of Shiga toxin-converting
893 bacteriophages in Escherichia coli. *J Bacteriol* **195**, 5007-5015 (2013).
894 https://doi.org/10.1128/JB.00592-13
895 10 Bryan, D., El-Shibiny, A., Hobbs, Z., Porter, J. & Kutter, E. M. Bacteriophage T4
896 Infection of Stationary Phase E. coli: Life after Log from a Phage Perspective. *Front*
897 *Microbiol* **7**, 1391 (2016). https://doi.org/10.3389/fmicb.2016.01391
898 11 Tabib-Salazar, A. *et al.* T7 phage factor required for managing RpoS in Escherichia
899 coli. *Proc Natl Acad Sci U S A* **115**, E5353-E5362 (2018).
900 https://doi.org/10.1073/pnas.1800429115
901 12 Zhang, T. *et al.* Direct activation of a bacterial innate immune system by a viral capsid
902 protein. *Nature* **612**, 132-140 (2022). https://doi.org/10.1038/s41586-022-05444-z
903 13 Jimmy, S. *et al.* A widespread toxin-antitoxin system exploiting growth control via
904 alarmone signaling. *Proc Natl Acad Sci U S A* **117**, 10500-10510 (2020).
905 https://doi.org/10.1073/pnas.1916617117
906 14 Kurata, T. *et al.* RelA-SpoT Homolog toxins pyrophosphorylate the CCA end of tRNA
907 to inhibit protein synthesis. *Mol Cell* **81**, 3160-3170 e3169 (2021).
908 https://doi.org/10.1016/j.molcel.2021.06.005
909 15 Zhang, T. *et al.* A bacterial immunity protein directly senses two disparate phage
910 proteins. *Nature* **635**, 728-735 (2024). https://doi.org/10.1038/s41586-024-08039-y
911 16 Ho, P. *et al.* Bacteriophage antidefense genes that neutralize TIR and STING immune
912 responses. *Cell Rep* **42**, 112305 (2023). https://doi.org/10.1016/j.celrep.2023.112305

913 17 Niault, T., van Houte, S., Westra, E. & Swarts, D. C. Evolution and ecology of anti-
914 defence systems in phages and plasmids. *Curr Biol* **35**, R32-R44 (2025).
915 https://doi.org/10.1016/j.cub.2024.11.033
916 18 Murtazalieva, K., Mu, A., Petrovskaya, A. & Finn, R. D. The growing repertoire of
917 phage anti-defence systems. *Trends Microbiol* **32**, 1212-1228 (2024).
918 https://doi.org/10.1016/j.tim.2024.05.005
919 19 Haseltine, W. A. & Block, R. Synthesis of guanosine tetra- and pentaphosphate
920 requires the presence of a codon-specific, uncharged transfer ribonucleic acid in the
921 acceptor site of ribosomes. *Proc Natl Acad Sci U S A* **70**, 1564-1568 (1973).
922 https://doi.org/10.1073/pnas.70.5.1564
923 20 Xiao, H. *et al.* Residual guanosine 3',5'-bispyrophosphate synthetic activity of relA
924 null mutants can be eliminated by spoT null mutations. *J Biol Chem* **266**, 5980-5990
925 (1991).
926 21 Fernández-Coll, L. & Cashel, M. Possible Roles for Basal Levels of (p)ppGpp: Growth
927 Efficiency Vs. Surviving Stress. *Front Microbiol* **11**, 592718 (2020).
928 https://doi.org/10.3389/fmicb.2020.592718
929 22 Vinella, D., Albrecht, C., Cashel, M. & D'Ari, R. Iron limitation induces SpoT-
930 dependent accumulation of ppGpp in Escherichia coli. *Mol Microbiol* **56**, 958-970
931 (2005). https://doi.org/10.1111/j.1365-2958.2005.04601.x
932 23 Spira, B., Silberstein, N. & Yagil, E. Guanosine 3',5'-bispyrophosphate (ppGpp)
933 synthesis in cells of Escherichia coli starved for Pi. *J Bacteriol* **177**, 4053-4058 (1995).
934 https://doi.org/10.1128/jb.177.14.4053-4058.1995
935 24 Ross, W., Vrentas, C. E., Sanchez-Vazquez, P., Gaal, T. & Gourse, R. L. The magic spot:
936 a ppGpp binding site on E. coli RNA polymerase responsible for regulation of
937 transcription initiation. *Mol Cell* **50**, 420-429 (2013).
938 https://doi.org/10.1016/j.molcel.2013.03.021
939 25 Ross, W. *et al.* ppGpp Binding to a Site at the RNAP-DksA Interface Accounts for Its
940 Dramatic Effects on Transcription Initiation during the Stringent Response. *Mol Cell*
941 **62**, 811-823 (2016). https://doi.org/10.1016/j.molcel.2016.04.029
942 26 Sanchez-Vazquez, P., Dewey, C. N., Kitten, N., Ross, W. & Gourse, R. L. Genome-wide
943 effects on Escherichia coli transcription from ppGpp binding to its two sites on RNA
944 polymerase. *Proceedings of the National Academy of Sciences* **116**, 8310-8319
945 (2019). https://doi.org/doi:10.1073/pnas.1819682116
946 27 Durfee, T., Hansen, A. M., Zhi, H., Blattner, F. R. & Jin, D. J. Transcription profiling of
947 the stringent response in Escherichia coli. *J Bacteriol* **190**, 1084-1096 (2008).
948 https://doi.org/10.1128/JB.01092-07
949 28 Traxler, M. F. *et al.* The global, ppGpp-mediated stringent response to amino acid
950 starvation in Escherichia coli. *Molecular microbiology* **68**, 1128-1148 (2008).
951 https://doi.org/10.1111/j.1365-2958.2008.06229.x
952 29 Bae, B. *et al.* Phage T7 Gp2 inhibition of Escherichia coli RNA polymerase involves
953 misappropriation of sigma70 domain 1.1. *Proceedings of the National Academy of*
954 *Sciences* **110**, 19772-19777 (2013). https://doi.org/doi:10.1073/pnas.1314576110
955 30 Severinova, E. & Severinov, K. Localization of the Escherichia coli RNA polymerase
956 beta' subunit residue phosphorylated by bacteriophage T7 kinase Gp0.7. *J Bacteriol*
957 **188**, 3470-3476 (2006). https://doi.org/10.1128/jb.188.10.3470-3476.2006

31 Savalia, D., Robins, W., Nechaev, S., Molineux, I. & Severinov, K. The role of the T7 Gp2 inhibitor of host RNA polymerase in phage development. *J Mol Biol* **402**, 118-126 (2010). https://doi.org/10.1016/j.jmb.2010.07.012

32 Sarubbi, E., Rudd, K. E. & Cashel, M. Basal ppGpp level adjustment shown by new spoT mutants affect steady state growth rates and rrnA ribosomal promoter regulation in Escherichia coli. *Molecular and General Genetics MGG* **213**, 214-222 (1988). https://doi.org/10.1007/BF00339584

33 Grucela, P. K. & Zhang, Y. E. Basal level of ppGpp coordinates Escherichia coli cell heterogeneity and ampicillin resistance and persistence. *Microb Cell* **10**, 248-260 (2023). https://doi.org/10.15698/mic2023.11.808

34 Gray Michael, J. Inorganic Polyphosphate Accumulation in Escherichia coli Is Regulated by DksA but Not by (p)ppGpp. *Journal of Bacteriology* **201**, 10.1128/jb.00664-00618 (2019). https://doi.org/10.1128/jb.00664-18

35 Gray Michael, J. Interactions between DksA and Stress-Responsive Alternative Sigma Factors Control Inorganic Polyphosphate Accumulation in Escherichia coli. *Journal of Bacteriology* **202**, 10.1128/jb.00133-00120 (2020). https://doi.org/10.1128/jb.00133-20

36 Zhang, Y. E. *et al.* (p)ppGpp Regulates a Bacterial Nucleosidase by an Allosteric Two-Domain Switch. *Mol Cell* **74**, 1239-1249.e1234 (2019). https://doi.org/10.1016/j.molcel.2019.03.035

37 Grucela, P. K., Fuhrer, T., Sauer, U., Chao, Y. & Zhang, Y. E. Ribose 5-phosphate: the key metabolite bridging the metabolisms of nucleotides and amino acids during stringent response in Escherichia coli? *Microb Cell* **10**, 141-144 (2023). https://doi.org/10.15698/mic2023.07.799

38 Wang, B. *et al.* Affinity-based capture and identification of protein effectors of the growth regulator ppGpp. *Nat Chem Biol* **15**, 141-150 (2019). https://doi.org/10.1038/s41589-018-0183-4

39 Wang, B., Grant, R. A. & Laub, M. T. ppGpp Coordinates Nucleotide and Amino-Acid Synthesis in E. coli During Starvation. *Mol Cell* **80**, 29-42.e10 (2020). https://doi.org/10.1016/j.molcel.2020.08.005

40 Maffei, E. *et al.* Systematic exploration of Escherichia coli phage-host interactions with the BASEL phage collection. *PLoS Biol* **19**, e3001424 (2021). https://doi.org/10.1371/journal.pbio.3001424

41 Qimron, U., Kulczyk, A. W., Hamdan, S. M., Tabor, S. & Richardson, C. C. Inadequate inhibition of host RNA polymerase restricts T7 bacteriophage growth on hosts overexpressing udk. *Mol Microbiol* **67**, 448-457 (2008). https://doi.org/10.1111/j.1365-2958.2007.06058.x

42 Kingston, R. E., Nierman, W. C. & Chamberlin, M. J. A direct effect of guanosine tetraphosphate on pausing of Escherichia coli RNA polymerase during RNA chain elongation. *Journal of Biological Chemistry* **256**, 2787-2797 (1981). https://doi.org/https://doi.org/10.1016/S0021-9258(19)69683-3

43 Tabib-Salazar, A. & Wigneshweraraj, S. RNA Management During T7 Infection. *Phage (New Rochelle)* **3**, 136-140 (2022). https://doi.org/10.1089/phage.2022.0029

44 Rodnina, M. V. Translation in Prokaryotes. *Cold Spring Harb Perspect Biol* **10** (2018). https://doi.org/10.1101/cshperspect.a032664

45 Casjens, S. R. The DNA-packaging nanomotor of tailed bacteriophages. *Nat Rev Microbiol* **9**, 647-657 (2011). https://doi.org/10.1038/nrmicro2632

46 Stano, N. M. & Patel, S. S. T7 lysozyme represses T7 RNA polymerase transcription by destabilizing the open complex during initiation. *J Biol Chem* **279**, 16136-16143 (2004). https://doi.org/10.1074/jbc.M400139200

47 Zhang, X. & Studier, F. W. Multiple Roles of T7 RNA Polymerase and T7 Lysozyme During Bacteriophage T7 Infection. *Journal of Molecular Biology* **340**, 707-730 (2004). https://doi.org/https://doi.org/10.1016/j.jmb.2004.05.006

48 Borges, A. & Athukoralage, J. *Phage amplification and concentration*, <https://www.protocols.io/view/phage-amplification-and-concentration-yxmvmnb86g3p/v1/references> (2022).

49 Ceelen, M. *Plaque assay*, <https://www.protocols.io/view/plaque-assay-kqdg35ebqv25/v1> (2019).

50 Kitagawa, M. *et al.* Complete set of ORF clones of Escherichia coli ASKA library (A Complete Set of E. coli K-12 ORF Archive): Unique Resources for Biological Research. *DNA Research* **12**, 291-299 (2006). https://doi.org/10.1093/dnares/dsi012

51 Baba, T. *et al.* Construction of Escherichia coli K-12 in-frame, single-gene knockout mutants: the Keio collection. *Mol Syst Biol* **2**, 2006.0008 (2006). https://doi.org/10.1038/msb4100050

52 Thomason, L. C., Costantino, N. & Court, D. L. E. coli genome manipulation by P1 transduction. *Curr Protoc Mol Biol* **Chapter 1**, 1 17 11-11 17 18 (2007). https://doi.org/10.1002/0471142727.mb0117s79

53 Cherepanov, P. P. & Wackernagel, W. Gene disruption in Escherichia coli: TcR and KmR cassettes with the option of Flp-catalyzed excision of the antibiotic-resistance determinant. *Gene* **158**, 9-14 (1995). https://doi.org/10.1016/0378-1119(95)00193-a

54 Varik, V., Oliveira, S. R. A., Hauryliuk, V. & Tenson, T. HPLC-based quantification of bacterial housekeeping nucleotides and alarmone messengers ppGpp and pppGpp. *Sci Rep* **7**, 11022 (2017). https://doi.org/10.1038/s41598-017-10988-6

55 Nozaki, S. & Niki, H. Exonuclease III (XthA) Enforces In Vivo DNA Cloning of Escherichia coli To Create Cohesive Ends. *J Bacteriol* **201** (2019). https://doi.org/10.1128/jb.00660-18

56 Liu, Y. *et al.* Basal ppGpp regulation by SpoT coordinates metabolic homeostasis and acid resistance. *bioRxiv*, 2026.2001.2026.700336 (2026). https://doi.org/10.64898/2026.01.26.700336

57 Zhang, Y., Zborníková, E., Rejman, D. & Gerdes, K. Novel (p)ppGpp Binding and Metabolizing Proteins of Escherichia coli. *mBio* **9** (2018). https://doi.org/10.1128/mBio.02188-17